ChemPubSoc Europe

DOI: 10.1002/ejic.201600427

EurJIC European Journal of Inorganic Chemistry

Full Paper

Vanadium Haloperoxidase Models

Vanadium Complexes Derived from Acetyl Pyrazolone and Hydrazides: Structure, Reactivity, Peroxidase Mimicry and Efficient Catalytic Activity for the Oxidation of 1-Phenylethanol

Mannar R. Maurya,*[a] Bithika Sarkar,[a] Fernando Avecilla,[b] and Isabel Correia*[c]

Abstract: Schiff bases obtained from the condensation of acetylpyrazolone (H_2ap) with benzoyl hydrazide (bhz), furoyl hydrazide (fah), nicotinoyl hydrazide (nah) and isonicotinoyl hydrazide (inh) [H_2ap-bhz (**I**), H_2ap-fah (**II**) H_2ap-nah, (**III**) and H_2ap-inh (**IV**)], sharing a ONO donor set, upon reaction with [$V^{IV}O(acac)_2$] lead to the formation of [$V^{IV}O$(ap-bhz)(H_2O)] (**1**), [$V^{IV}O$(ap-fah)(H_2O)] (**2**), [$V^{IV}O$(ap-nah)(H_2O)] (**3**) and [$V^{IV}O$(ap-inh)(H_2O)] (**4**), respectively. These complexes slowly convert to monooxidovanadium(V) complexes [$V^{V}O$(ap-bhz)(OMe)(MeOH)] (**11**), [$V^{V}O$(ap-fah)(OMe)(MeOH)] (**12**), [$V^{V}O$(ap-nah)(OMe)(MeOH)] (**13**) and [$V^{V}O$(ap-inh)(OMe)(MeOH)] (**14**) in methanol. The reaction of aqueous K[$H_2V^{V}O_4$] with the corresponding potassium salt of the ligands at neutral pH gives dioxidovanadium(V) complexes, K(H_2O)[$V^{V}O_2$(ap-bhz)] (**5**), K(H_2O)$_{0.5}$[$V^{V}O_2$(ap-fah)] (**6**), [$V^{V}O_2$(Hap-nah)] (**9**) and [$V^{V}O_2$(Hap-nah)] (**10**). Acidification of solutions of **5** and **6** affords the neutral complexes [$V^{V}O_2$(Hap-bhz)] (**7**) and [$V^{V}O_2$(Hap-fah)] (**8**), respectively. All complexes were characterized by various spectroscopic techniques: FT-IR, UV/Visible, EPR, NMR (^{1}H, ^{13}C and ^{51}V); elemental analysis, thermal studies, cyclic voltammetry (CV) and single-crystal X-ray analysis. X-ray diffraction studies of complexes **6**, **7**, **9**–**12** confirm the ligand's coordination to the metal centre through enolic oxygen (of pyrazolone), azomethine nitrogen and enolic oxygen (hydrazide) atoms. The reactivity of the complexes and their catalytic potential was screened towards their peroxidase mimetic activity in the oxidation of pyragallol in aqueous media with H_2O_2 as oxidant, showing high activity under mild conditions. They were also tested in the catalytic oxidation of 1-phenylethanol with H_2O_2 that yields acetophenone as main product. Parameters such as catalyst and oxidant amount, time, temperature, and solvent effects were optimised for maximum oxidation of 1-phenylethanol. The complexes show excellent catalytic activity towards oxidation of 1-phenylethanol being structural and functional models of the vanadate-dependent haloperoxidases.

Introduction

Peroxidases catalyse the oxidation of a broad range of substrates, using H_2O_2 or other peroxides as oxidants. They have been successfully applied in different fields such as medicine, chemical industries, food processing, treatment of industrial waste and agriculture.[1] However, peroxidases have some intrinsic drawbacks associated with their denaturation, special storage requirements and cost. In current years artificial enzyme mimics have become a hot topic of research[2] since they present many advantages over conventional enzymes, namely easier preparation, lower price and improved stability, overcoming the drawbacks of natural enzymes.[3–5] At present, a large number of artificial enzymes have been synthesized by incorporating a catalytic centre into a variety of scaffolds including ligand-anchoring supramolecular complexes,[6] Schiff base complexes,[7] hemes,[8] porphyrins,[9] micelles,[10] vesicles,[11] nanoparticles,[12] and nanorods.[13]

In the last several decades, a high number of vanadium complexes have been synthesized and characterized due to continued interest in the bioinorganic chemistry of vanadium, as recognized by several monographs.[14] Vanadium complexes with biologically important ligands, aiming to find structural and/or functional models of biogenic compounds are numerous and have been reported in several reviews.[15] Our group has made several contributions in recent years to the field of peroxidase mimics.[16]

In continuation of our efforts we report herein the synthesis of oxidovanadium(IV), oxidovanadium(V) and dioxidovanadium(V) complexes of pyrazolone derivatives; Scheme 1. Pyrazolone ligands and their derivatives have shown biological and therapeutical properties, such as antitumor, antimicrobial, and antiviral activities,[17] however, their chemistry and applications are still underexplored. Recently, we reported the synthesis of tridentate ONO donor ligands derived from a pyrazolone (4-acetyl-3-methyl-1-phenyl-2-pyrazoline-5-one, Hap) and aromatic hydrazides along with the application of their molybdenum complexes[18] as catalysts for dynamic covalent assem-

[a] *Department of Chemistry, Indian Institute of Technology Roorkee, 247667Roorkee, India*
E-mail: rkmanfcy@iitr.ac.in
www.iitr.ac.in/~CY/rkmanfcy
[b] *Departamento de Química Fundamental, Universidade da Coruña, Campus de A Zapateira, 15071 A Coruña, Spain*
[c] *Centro de Química Estrutural, Instituto Superior Técnico, Universidade de Lisboa, Av. Rovisco Pais 1, 1049-001 Lisbon, Portugal*

Supporting information for this article is available on the WWW under http://dx.doi.org/10.1002/ejic.201600427.

blies, via Hantzsch reaction, using 30 % H_2O_2 as oxidant, under solvent free conditions. We extend this study by evaluating the peroxidase mimetic activity of the vanadium complexes of pyrazolone-based ligands, using the oxidation of pyrogallol with H_2O_2 as model reaction.

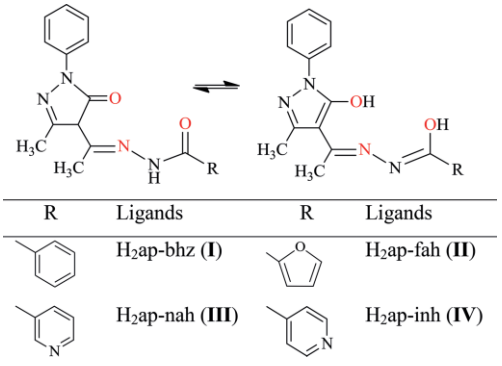

R	Ligands	R	Ligands
	H_2ap-bhz (**I**)		H_2ap-fah (**II**)
	H_2ap-nah (**III**)		H_2ap-inh (**IV**)

Scheme 1. Structural formulae of ligands. Keto-enol tautomerism of a general structure of hydrazones is also shown here.

To extend the scope, the oxidation of 1-phenylethanol to acetophenone has also been carried out, giving further support to the peroxidase mimetic activity of the reported complexes. This is a particularly relevant reaction since the controlled oxidation of alcohols to the corresponding carbonyl compounds, is a fundamental transformation of enormous importance. Although, there are many known stoichiometric oxidation methods, e.g. by pyridinium chlorochromate (PCC), Swern type, Dess–Martin periodinane and Oppenauer type, for economic and environmental reasons, the development of efficient and selective catalysts for such an oxidation is a demanding field of study in the chemical industry.[19]

Results and Discussion

Synthesis, Characterization and Reactivity of the Complexes

Precursor $[V^{IV}O(acac)_2]$ reacts with equimolar amounts of ligands H_2ap-bhz (**I**), H_2ap-fah (**II**) H_2ap-nah (**II**) and H_2ap-inh (**IV**) in refluxing 95 % methanol to give oxidovanadium(IV) complexes, $[V^{IV}O(ap\text{-}bhz)(H_2O)]$ (**1**), $[V^{IV}O(ap\text{-}fah)(H_2O)]$ (**2**), $[V^{IV}O(ap\text{-}nah)(H_2O)]$ (**3**) and $[V^{IV}O(ap\text{-}inh)(H_2O)]$ (**4**), respectively, [Equation (1) considering H_2ap-bhz (**I**) as representative ligand].

$$[V^{IV}O(acac)_2] + H_2ap\text{-}bhz + H_2O \rightarrow [V^{IV}O(ap\text{-}bhz)(H_2O)] + 2Hacac \quad (1)$$

Crystallisation over the course of a week along with aerial oxidation of these complexes in MeOH, results in the formation of $[V^{V}O(L)(OMe)(MeOH)]$ (**11**–**14**) [Equation (2), considering complex **1** as representative].

$$2[V^{IV}O(ap\text{-}bhz)(H_2O)] + 1/2\ O_2 + 4\ MeOH \rightarrow 2[V^{V}O(ap\text{-}bhz)(OMe)(MeOH)] + 3H_2O \quad (2)$$

A solution of potassium vanadate (which, at pH 7 is predominantly $K[H_2VO_4]$),[20] generated in situ by dissolving V_2O_5 in aqueous KOH, reacts with ligands H_2ap-bhz (**I**) and H_2ap-fah (**II**) at pH ca. 7.0 to give the potassium salts of the corresponding dioxidovanadium(V) anions, $K(H_2O)[V^{V}O_2(ap\text{-}bhz)]$ (**5**) and $K(H_2O)_{0.5}[V^{V}O_2(ap\text{-}fah)]$ (**6**) [Equation (3) considering complex **5** as representative]. Under similar reaction conditions, neutral complexes $[V^{V}O_2(Hap\text{-}nah)]$ (**9**) and $[V^{V}O_2(Hap\text{-}inh)]$ (**10**) [Equation (4)] were obtained from ligands H_2ap-nah (**III**) and H_2ap-inh (**IV**). In these complexes the pyridinic nitrogen undergoes protonation helping to stabilize the complexes in their neutral forms.

$$K[H_2VO_4] + K_2ap\text{-}bhz + 2HCl \rightarrow [K(H_2O)][V^{V}O_2(ap\text{-}bhz)] + 2KCl + H_2O \quad (3)$$

$$K[H_2VO_4] + K_2L + 3HCl \rightarrow [V^{V}O_2HL] + 3KCl + 2H_2O\ (H_2L = \textbf{III}: \textbf{9};\ H_2L = \textbf{IV}: \textbf{10}) \quad (4)$$

Complexes, $K(H_2O)[V^{V}O_2(ap\text{-}bhz)]$ (**5**) and $K(H_2O)_{0.5}[V^{V}O_2(ap\text{-}fah)]$ (**6**) could also be converted into $[V^{V}O_2(Hap\text{-}bhz)]$ (**7**) and $[V^{V}O_2(Hap\text{-}fah)]$ (**8**), respectively, by reacting their methanolic solutions with aqueous HCl [Equation (5) considering complex **5** as a representative]. These two complexes have the ligand coordinated in the ketonic (hydrazide) form.

$$K(H_2O)[V^{V}O_2(ap\text{-}bhz)] + HCl \rightarrow [V^{V}O_2(Hap\text{-}bhz)] + KCl + H_2O \quad (5)$$

Scheme 2 provides an overview of the complexes discussed in this paper. The structural formulae proposed are based on elemental analyses, spectroscopic data (IR, UV/Vis, EPR, ^1H, ^{13}C and ^{51}V NMR) and thermal studies. Structures of complexes **6**, **7**, **9**–**12** have been further validated by single-crystal X-ray diffraction studies. All complexes exist as monomers and are soluble in methanol, ethanol, acetonitrile, DMF, and DMSO, to differing extents.

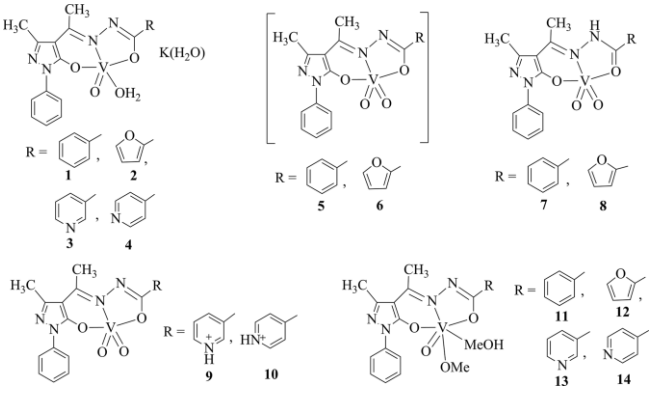

Scheme 2. Overview of the complexes described in this work.

Thermal Analysis

The thermal stability of the complexes was studied under oxygen atmosphere and relevant data is presented in Table S1 (Supporting Information). Complexes **1**–**4** are thermally stable up to ca. 100 °C. Above this temperature, **1**–**4** lose masses roughly equal to one water molecule, indicating the presence of weekly coordinated water. The anhydrous complexes decompose between 200 to 490 °C in three overlapping steps; the final decomposition product is V_2O_5. Complexes **5** and **6** both

lose a mass equal to one water molecule in the temperature range 120–190 °C, which is attributed to the coordinated water molecule. The water-free species starts to decompose with multiple exothermic, but overlapping, steps upon further increasing the temperature; these steps are complete above ca. 550 °C, giving KVO_3 as the final product. Complexes **7**–**10** are stable up to ca. 550 °C. Beyond this temperature they start to decompose exothermically to give V_2O_5 as the final product. Complexes **11**–**14** each undergo mass loss roughly equivalent to one methanol molecule in the temperature range 90–160 °C, confirming the presence of a coordinated MeOH. Further increasing the temperature, results in mass loss roughly equivalent to one methoxido (–OMe) group, indicating the presence of one coordinated –OMe group. These complexes decompose giving the final product V_2O_5 in the temperature range ca. 470–500 °C.

X-ray Diffraction Studies

Table 1 provides selected bond lengths and angles for all compounds. Compound $\{K(H_2O)_{0.25}[V^VO_2(ap\text{-}fah)]\}_n$ (**6**) crystallized from methanol as orange blocks and Figure 1 (A) depicts an ORTEP representation of the asymmetric unit. In the solid state the compound presents a polymeric structure with electrostatic interactions between V=O bonds and potassium atoms. The asymmetric unit of **6** contains a mononuclear vanadium complex with the ligand, ap-fah, one potassium atom and 0.25 water molecules interacting with potassium atoms. The coordination polyhedron around the K ions can be best described as a distorted dodecahedron with triangular faces [see Figure 1 (B)], with the water molecule occupying only occasionally the eighth coordination site. In the crystal packing of **6**, presented in Figure S1 (Supporting Information), the heteroatoms are seen to interact electrostatically. The crystal packing can be described as layers of vanadium complexes with the K ions occupying positions between layers. Each vanadium centre is five-coordinated. Since $\alpha_{N3-V1-O4}$ = 143.95° and $\beta_{O2-V1-O3}$ = 148.89°, the τ value of 0.08 [$\tau = (\beta-\alpha)/60$] indicates a slightly distorted square pyramidal geometry.[21] Each vanadium centre is coordinated to the ligand through the enolic oxygen (of pyrazolone) atom [V1–O2, 1.9462(13) Å], azomethine nitrogen atom, [V1–N3, 2.1741(15) Å] and one oxygen atom of hydrazide group [V1–O3, 1.9411(13) Å]. The coordination sphere is completed by two oxygen atoms [V1–O4, 1.6388(13) Å and V1–O1, 1.6266(14) Å], which interact with the potassium atoms. The pyrazolone group (C1, C2, C3, N1, N2) and furan of the hydrazide group (C14, C15, C16, C17, O5) are coplanar [mean deviation from planarity, 0.0110(15) Å], and the other benzyl group (C7, C8, C9, C10, C11, C12) forms a torsion angle of 16.19(08)° over the previous coplanar rings. The vanadium atoms are displaced toward the apical oxido ligand (O1) from the equatorial plane defined by the O2, O3, O4 and N3 atoms, 0.5120(7) Å, [mean deviation from planarity, O2, O3, O4, N3, 0.0603(7) Å]. The two oxygen atoms present V=O bonds characteristic of oxido-type O atoms with strong π bonding.[23] The V–K separations, which depend on the position of the potassium ion in the crystal packing are 3.4721(5) Å and 3.6466(5) Å.

Table 1. Bond lengths [Å] and angles [°] for $\{K(H_2O)_{0.25}[V^VO_2(ap\text{-}fah)]\}_n$ (**6**), $[V^VO_2(Hap\text{-}bhz)]\cdot H_2O$ (**7**), $[V^VO_2(Hap\text{-}nah)]$ (**9**), $[V^VO_2(Hap\text{-}inh)]\cdot H_2O$ (**10**), $[V^VO(ap\text{-}bhz)(OMe)(MeOH)]$ (**11**) and $[V^VO(ap\text{-}fah)(OMe)(MeOH)]$ (**12**).[a]

Bond lengths	**6**	**7**	**9**
V(1)–O(1)	1.6266(14)	1.614(2)	1.6078(16)
V(1)–O(2)	1.9462(13)	1.9289(18)	1.9558(14)
V(1)–O(3)	1.9411(13)	1.9436(19)	1.9184(13)
V(1)–O(4)	1.6388(13)	1.636(2)	1.6572(15)
V(1)–O(5)			
V(1)–N(3)	2.1741(15)	2.187(2)	2.1683(16)
V(1)–K(1)#1	3.4721(5)		
V(1)–K(1)#2	3.6466(5)		
K(1)–O(4)#3	2.6686(13)		
K(1)–O(1)	2.7094(14)		
K(1)–O(5)#4	2.7159(14)		
K(1)–O(1)#1	2.8161(14)		
K(1)–O(4)#1	2.8301(13)		
K(1)–O(1 W)	2.896(10)		
K(1)–O(2)#3	2.9302(13)		
K(1)–N(4)#4	2.9956(16)		
K(1)–V(1)#1	3.4721(5)		
K(1)–V(1)#3	3.6466(5)		
K(1)–K(1)#1	4.2740(8)		
O(1)–K(1)#1	2.8161(14)		
Angles	**6**	**7**	**9**
O(1)–V(1)–O(5)			
O(1)–V(1)–O(2)	103.87(6)	104.66(9)	103.46(7)
O(5)–V(1)–O(2)			
O(1)–V(1)–O(3)	104.01(7)	103.48(10)	103.40(7)
O(5)–V(1)–O(3)			
O(2)–V(1)–O(3)	148.80(6)	146.75(9)	149.09(6)
O(1)–V(1)–N(3)	109.10(6)	100.82(10)	104.55(7)
O(5)–V(1)–N(3)			
O(2)–V(1)–N(3)	83.50(5)	83.39(8)	74.38(6)
O(3)–V(1)–N(3)	74.37(6)	74.22(8)	84.29(6)
O(1)–V(1)–O(4)	106.61(7)	109.87(12)	110.49(9)
O(5)–V(1)–O(4)			
O(2)–V(1)–O(4)	92.78(6)	94.80(9)	91.39(7)
O(3)–V(1)–O(4)	92.44(6)	92.00(9)	93.33(6)
N(3)–V(1)–O(4)	143.95(6)	148.63(11)	144.42(8)
Bond lengths	**10**	**11**	**12**
V(1)–O(1)	1.639(5)	1.5887(13)	1.665(4)
V(1)–O(2)	1.980(5)	1.9216(16)	2.000(4)
V(1)–O(3)	1.959(4)	1.9133(16)	2.005(4)
V(1)–O(4)	1.652(4)	2.2572(14)	2.429(4)
V(1)–O(5)		1.7654(13)	1.847(4)
V(1)–N(3)	2.213(5)	2.1618(15)	2.256(4)
Angles	**10**	**11**	**12**
O(1)–V(1)–O(5)		101.68(7)	100.92(19)
O(1)–V(1)–O(2)	103.33(16)	98.42(7)	97.3(2)
O(5)–V(1)–O(2)		98.82(6)	97.73(17)
O(1)–V(1)–O(3)	104.51(17)	99.38(7)	97.9(2)
O(5)–V(1)–O(3)		95.12(6)	95.91(16)
O(2)–V(1)–O(3)	146.96(17)	154.63(6)	157.26(17)
O(1)–V(1)–N(3)	100.57(18)	94.34(6)	97.44(19)
O(5)–V(1)–N(3)		162.65(6)	160.39(18)
O(2)–V(1)–N(3)	73.83(14)	85.25(6)	86.66(14)
O(3)–V(1)–N(3)	83.85(14)	75.52(6)	74.67(14)
O(1)–V(1)–O(4)		175.01(6)	175.91(17)
O(5)–V(1)–O(4)		83.31(6)	83.17(16)
O(2)–V(1)–O(4)	92.37(15)	80.84(6)	82.18(16)
O(3)–V(1)–O(4)	94.27(15)	79.85(6)	81.47(16)
N(3)–V(1)–O(4)	148.3(2)	80.69(6)	78.49(15)

[a] Symmetry transformations used to generate equivalent atoms: #1 –*x*, –*y* + 1, –*z* + 1; #2 *x*,*y*,*z*+1; #3 *x*, *y*, *z* – 1; #4 –*x* + 1, –*y* + 1, –*z* + 1.

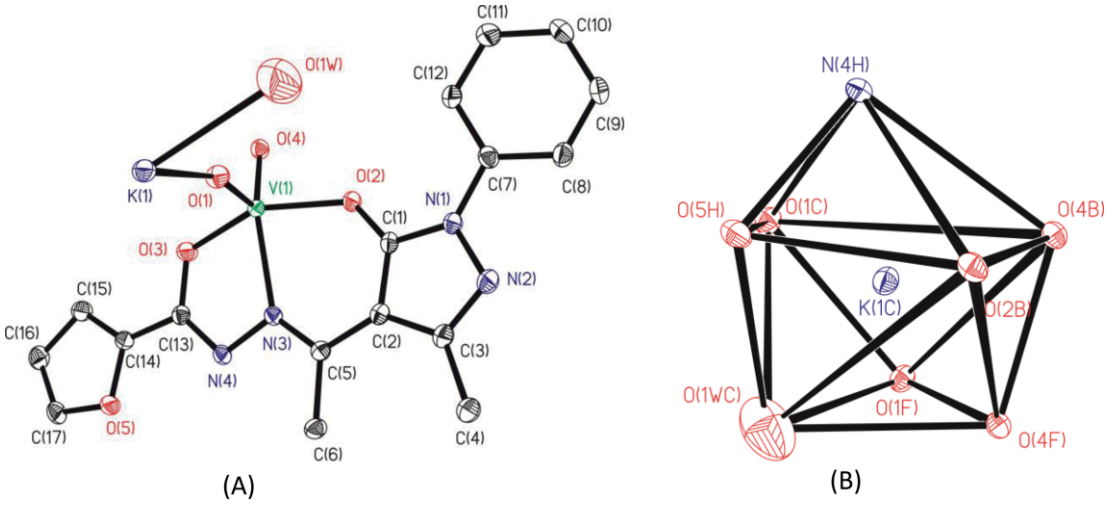

Figure 1. (A) Asymmetric unit of compound $\{K(H_2O)_{0.25}[V^VO_2(ap\text{-}fah)]\}_n$ (**6**). All the non-hydrogen atoms are presented by their 50 % probability ellipsoids. Hydrogen atoms are omitted for clarity. (B) Coordination polyhedron around K ion in **6**.

Compounds $[V^VO_2(Hap\text{-}bhz)]\cdot H_2O$ (**7**), $[V^VO_2(Hap\text{-}nah)]$ (**9**) and $[V^VO_2(Hap\text{-}inh)]\cdot H_2O$ (**10**) crystallized from methanol, methanol/ethanol and DMSO, respectively, as dark orange blocks and Figures 2, 3 and 4 depict ORTEP representations of the complexes in the asymmetric unit. These compounds contain mononuclear vanadium complexes with the ligands ap-bhz, ap-nah and ap-inh, protonated (compound **7** in the azomethine group and compound **9** and **10** in the pyridine group). Each vanadium centre is five-coordinate. For **7** ($\alpha_{N3-V1-O4}$ = 148.63°, $\beta_{O2-V1-O3}$ = 146.75°) the value τ = 0.031, for **9** ($\alpha_{N3-V1-O4}$ = 144.42°, $\beta_{O2-V1-O3}$ = 149.09°) τ = 0.078, and for **10** ($\alpha_{N3-V1-O4}$ = 148.3°, $\beta_{O2-V1-O3}$ = 146.96) τ = 0.022, all indicating distorted square pyramidal geometries.[22] Figures S2, S3 and S4 (Supporting Information), present the crystal packing of compounds **7**, **9** and **10**, respectively. The crystal packing can be described as layers of vanadium complexes, which interact by van der Waals forces and π–π stacking interactions. In compound **7**, the distance between centroids of phenyl groups, c1–c2 is 3.618(2) Å [c1, C(14O)–C(15O)–C(16O)–C(17O)–C(18O)–C(19O), c2, C(8N)–C(9N)–C(10N)–C(11N)–C(12N)–C(13N)]. In compound **9**, antiparallel π–π stacking interactions (Figure 5) occur between the pyrazolone groups. The distance between centroids, c3–c4, is 3.539(2) Å [c3, C(1C)–C(2C)–C(3C)–N(1C)-N(2C), c4, C(1O)–C(2O)–C(3O)–N(1O)-N(2O)]. In compound **10**, the distance between centroids of phenyl and pyridine groups, c5–c6, is 3.661(2) Å [c5, C(13C)–C(14C)–C(15C)–C(16C)–C(17C)–C(18C), c6, C(8B)–C(9B)–C(10B)–C(11B)–C(12B)-(N5B)]. Each vanadium centre is coordinated to the ligands through the enolic oxygen (of pyrazolone) atom [V1–O2, 1.9289(18) Å, in **7**, 1.9558(14) Å, in **9** and 1.980(5) Å in **10**], azomethine nitrogen atom, [V1–N3, 2.187(2) Å, in **7**, 2.1683(16) Å, in **9** and 2.213(5) Å in **10**] and one oxygen atom of the hydrazide group [V1–O3, 1.9436(19) Å, in **7**, 1.9184(13) Å, in **9** and 1.959(4) Å in **10**]. The coordination sphere is completed with two terminal oxido atoms [V1–O4, 1.636(2) Å in **7**, 1.6572(15) Å in **9** and 1.652(4) Å in **10** and V1–O1, 1.614(2) Å in **7**, 1.6078(16) Å in **9** and 1.639(5) Å in **10**]. The pyrazolone group (C1, C2, C3, N1, N2) and phenyl or pyridine of the hydrazide group (C8, C9, C10, C11, C12, C13 in **7**, C8, C9,

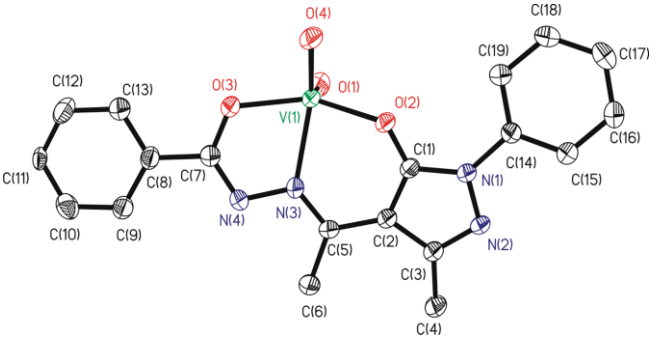

Figure 2. ORTEP plot of complex $[V^VO_2(Hap\text{-}bhz)]$ (**7**). All the non-hydrogen atoms are presented by their 50 % probability ellipsoids. Hydrogen atoms are omitted for clarity.

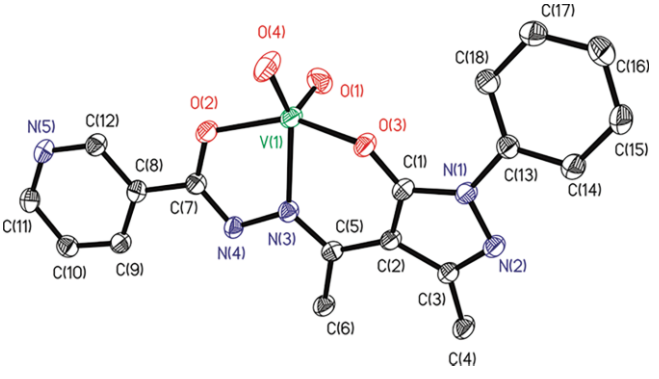

Figure 3. ORTEP plot of complex $[V^VO_2(Hap\text{-}nah)]$ (**9**). All the non-hydrogen atoms are presented by their 50 % probability ellipsoids. Hydrogen atoms are omitted for clarity.

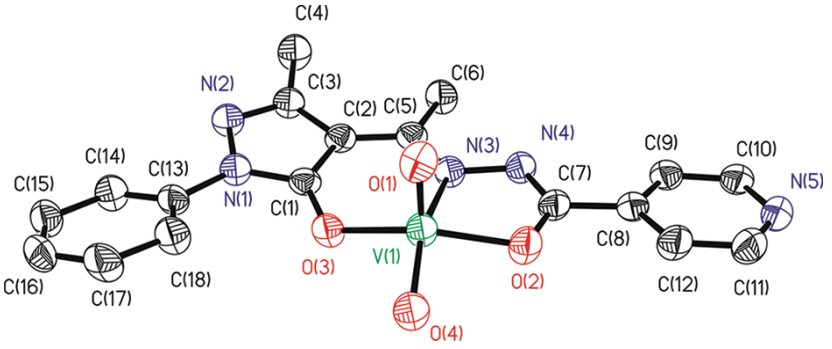

Figure 4. ORTEP plot of complex [$V^{V}O_2$(Hap-inh)] (**10**). All the non-hydrogen atoms are presented by their 50 % probability ellipsoids. Hydrogen atoms are omitted for clarity.

C10, C11 C12, N5 in **9** and **10**) are quasi-coplanar [mean deviation from planarity, 0.1093(22) Å in **7**, 0.0981(15) Å in **9** and 0.1095(41) Å in **10**], and the other phenyl group (C14, C15, C16, C17, C18, C19 in **7** and C13, C14, C15, C16, C17, C18 in **9** or **10**) forms a torsion angle of 12.19(9)° in **7**, 11.64(08)° in **9** and 12.42(29)° in **10**, over the previous coplanar rings. The vanadium atom is displaced towards the apical oxido ligand (O1) from the equatorial plane defined by the O2, O3, O4 and N3 atoms, 0.4886(11) Å in **7**, 0.5084(8) Å in **9** and 0.4966(20) Å in **10**, [mean deviation from planarity, O2, O3, O4, N3, 0.0069(11) Å in **7**, 0.0562(8) Å in **9** and 0.0098(20) Å in **10**]. The two terminal oxygen atoms present V=O bonds characteristic of oxido-type O atoms with strong π bonding.[22] Intermolecular hydrogen bonds appear between protonated pyridine and terminal oxygen atoms in compounds **9** and **10**.

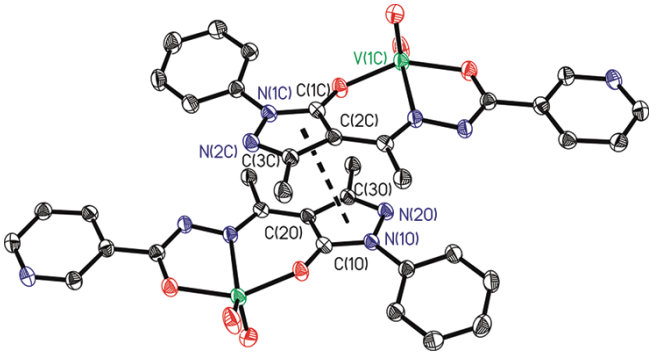

Figure 5. Antiparallel π–π stacking interactions present in the crystal packing of [$V^{V}O_2$(Hap-nah)] (**9**).

Compounds [V^{V}O(ap-bhz)(OMe)(MeOH)] (**11**) and [V^{V}O(ap-fah)(OMe)(MeOH)] (**12**) crystallized from methanol as black blocks and Figures 6 and 7 depict ORTEP representations of the asymmetric units. Both structures show mononuclear complexes with six-coordinate distorted octahedral geometry. The axial sites of the octahedron are occupied by the oxido O-atom and by one methanol molecule [V1–O1, 1.5887(13) Å, V1–O4, 2.2572(14) Å, in **11** and V1–O1, 1.665(4) Å, V1–O4, 2.429(4) Å, in **12**]. The other coordinated atoms form a plane [O2, O3, O5, N3, mean deviation from planarity, 0.0208(7) Å, in **11** and 0.0272(22) Å, in **12**] with the vanadium atom displaced towards the apical oxido ligand by 0.2904(7) Å in **11** and 0.2960(23) Å in **12**. In **11** the pyrazolone group (C1, C2, C3, N1, N2) and benzyl of hydrazide group (C8, C9, C10, C11, C12, C13) are coplanar [mean deviation from planarity, 0.1154(16) Å], and the other benzyl group (C14, C15, C16, C17, C18, C19) forms a torsion angle of 9.70(06)° over the previous coplanar rings. In **12** these values are: mean deviation from planarity, 0.0734(45) Å, and torsion angle of 23.74(23)°. The distances V1-$O_{enolates}$ [V1–O2, 1.9216(16) Å, and V1–O3, 1.9133(16) Å, in **11** and V1–O2, 2.000(4) Å, and V1–O3, 2.005(4) Å, in **12**] are higher than V1-$O_{methoxido}$ [V1–O5, 1.7654(13) Å, in **11** and 1.847(4) Å, in **12**].

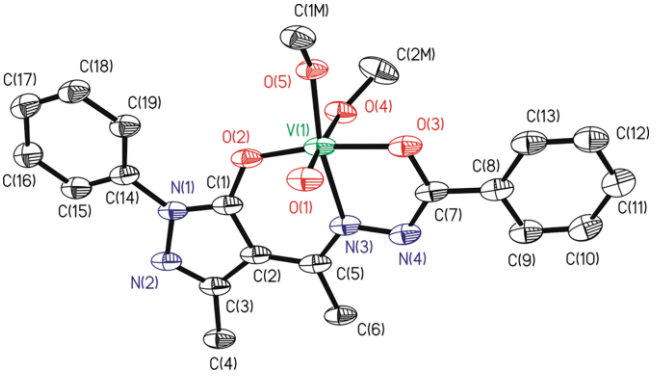

Figure 6. ORTEP plot of complex [V^{V}O(ap-bhz)(OMe)(MeOH)] (**11**). All the non-hydrogen atoms are presented by their 50 % probability ellipsoids. Hydrogen atoms are omitted for clarity.

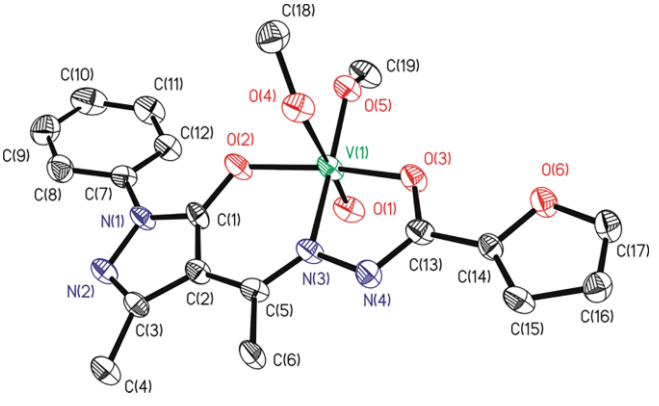

Figure 7. ORTEP plot of complex [V^{V}O(ap-fah)(OMe)(MeOH)] (**12**). All the non-hydrogen atoms are presented by their 50 % probability ellipsoids. Hydrogen atoms are omitted for clarity.

The bond length to the function *trans* to the oxido group (V1–O4) is somewhat elongated, as a consequence of the *trans* influence in the two compounds. In the crystal packing of compounds **11** and **12**, the layered structure present in compounds **6**, **7** and **9** is not observed, (see Figures S5 and S6, Supporting Information). Intermolecular hydrogen bonds appear between coordinated methanol groups and nitrogen atoms, N2, of pyrazolone groups, in **11** (see Table 2).

Table 2. Hydrogen bonds in compounds [$V^{V}O_2$(Hap-nah)] (**9**) and [V^{V}O-(ap-bhz)(OMe)(MeOH)] (**11**).[a]

D–H···A (compound)	*d*(D–H)	*d*(H···A)	*d*(D···A)	<(DHA)
N(5)–H(5N)···O(1)#1 (**9**)	0.95(3)	1.63(3)	2.563(2)	167(3)
O(4)–H(4)···N(2) #2 (**11**)	0.73(3)	2.02(3)	2.753(3)	172(3)

[a] Symmetry transformations used to generate equivalent atoms: #1 $-x+2$, $-y+1$, $-z+1$; #2 $-x$, $-y$, $-z+1$.

IR Spectral Studies

A partial list of IR spectroscopic data of the ligands and complexes is presented in Table S2 (Supporting Information). Bands appearing at 2970–2991 cm^{-1} and 1615–1646/1586–1595 cm^{-1} in the spectra of the ligands, due to the presence of υ(N–H) and υ(C=$O_{hydrazide/pyrazolone}$), are indicative of the ketonic nature of the ligands in the solid state. These bands disappear upon complex formation (except in **7** and **8**) due to enolization of the ketonic group and replacement of the H atom by the metal ion. A sharp band appearing in the region 1225–1250 cm^{-1} is assigned to the υ(C-O_{enolic}) mode. A strong band at 1540–1550 cm^{-1} in the spectra of ligands is assigned to ν(C=N) and this band shifts to lower wave numbers, by 20–25 cm^{-1} in the spectra of complexes, indicating coordination of the azomethine nitrogen. The ligand band assigned to υ(N-N) appearing at 976–979 cm^{-1} shifts to higher wave numbers, by 60–90 cm^{-1}, in the complexes, which further supports the azomethine coordination. The shift of the ν(N-N) band to higher frequency is expected because of the reduced repulsion between the lone pairs of adjacent nitrogen atoms. Complexes **7**–**10** exhibit a band at 3051–3071 cm^{-1}, which indicates that the hydrazine (in **7** and **8**) or the pyridinic nitrogen of the ring (in **9** and **10**) gets protonated during complexation. A broad band attributed to –OH appears at 2900–3000 cm^{-1} in the spectra of ligands, due to intramolecular hydrogen bonding. In the metal complexes this band is shifted to ca. 3410–3460 cm^{-1}, possibly due to the breaking of hydrogen bonding as well as coordination of water (in complexes **1**–**6**) and methanol molecules (in complexes **11**–**14**).

The $V^{IV}O$ complexes exhibit a sharp band at 976–989 cm^{-1} due to ν(V=O) stretch while in $V^{V}O$ complexes this band appears at 956–966 cm^{-1}. The dioxido $V^{V}O_2$ complexes exhibit two such sharp bands in the 896–938 cm^{-1} region due to ν_{sym}(O=V=O) and ν_{asym}(O=V=O) modes. These bands confirm the *cis*-$V^{V}O_2$ structure in these complexes.[15d]

Electronic Spectral Studies

Table 3 presents UV/Vis spectroscopic data of the ligands and the complexes measured in MeOH or DMSO. We recently reported spectral studies of the ligands, **I**–**IV**, and their dioxidomolybdenum(VI) complexes.[18] The spectra of the complexes in the UV region, reported here, follow very similar spectral patterns i.e. the $\varphi \rightarrow \varphi^*$, $\pi \rightarrow \pi_1^*$, $\pi \rightarrow \pi_2^*$, and $n \rightarrow \pi^*$ transitions observed in the spectra of ligands are slightly shifted in the corresponding spectra of complexes. In addition, a new band of medium intensity appears at ca. 390–402 nm, which is assigned to a ligand to metal charge transfer (LMCT) band. The $V^{IV}O$ complexes exhibit bands in the visible region, assigned to d–d transitions.

Table 3. UV/Visible spectroscopic data of ligands and vanadium complexes, either in MeOH or DMSO.

	Solvent	λ_{max}/nm (ε/M^{-1} cm^{-1})
H_2ap-bhz (**I**)	MeOH	347 (8.54×10^3), 281 (1.02×10^3), 248 (1.30×10^4), 227 (1.29×10^4), 205 (1.95×10^4)
H_2ap-fah (**II**)	MeOH	378 (8.76×10^3), 362 (9.26×10^3), 289 (1.11×10^4), 251 (1.61×10^4), 204 (1.43×10^4)
H_2ap-nah (**III**)	MeOH	375 (1.61×10^4), 279 (9.90×10^3), 249 (1.64×10^4), 201 (2.06×10^4)
H_2ap-inh (**IV**)	MeOH	385 (1.62×10^4), 283 (9.26×10^3), 250 (1.64×10^4), 203 (1.80×10^4)
[V^{IV}O(ap-bhz)H_2O] (**1**)	MeOH	636 (1.2×10^2), 395 (3.9×10^3), 368 (2.9×10^4), 240 (4.1×10^4), 201 (4.3×10^4)
	DMSO	610 (1.20×10^2), 374 (1.50×10^3)
[V^{IV}O(ap-fah)H_2O] (**2**)	MeOH	642 (3.4×10^2), 395 (4.8×10^3), 368 (4.1×10^4), 240 (4.1×10^4), 201 (4.8×10^4)
	DMSO	600 (30, sh), 375 (1.55×10^4)
[V^{IV}O(ap-nah)H_2O] (**3**)	MeOH	641(4.0×10^2), 393 (2.3×10^3), 342 (3.4×10^4), 233 (3.3×10^4), 203 (3.7×10^4)
	DMSO	744 (20), 533 (25, sh), 410 (8.00×10^3), 387 (1.32×10^4), 378 (1.36×10^4)
[V^{IV}O(ap-inh)H_2O] (**4**)	MeOH	645(2.3×10^2), 390 (4.1×10^3), 340 (3.2×10^4), 244 (4.8×10^4), 201 (4.8×10^4)
	DMSO	735 (40, sh), 419 (9.90×10^3), 388 (1.40×10^4), 381 (1.41×10^4)
K(H_2O)[$V^{V}O_2$(ap-bhz)] (**5**)	MeOH	396 (2.6×10^3), 324 (3.9×10^4), 243 (4.2×10^4), 202 (3.9×10^4)
K(H_2O)$_{0.5}$[$V^{V}O_2$(ap-fah)] (**6**)	MeOH	397 (3.1×10^3), 328 (2.8×10^4), 243 (3.5×10^4), 203 (2.8×10^4)
[$V^{V}O_2$ (Hap-bhz)] (**7**)	MeOH	395 (2.8×10^3), 328 (3.1×10^4), 243 (3.5×10^4), 203 (2.9×10^4)
[$V^{V}O_2$ (Hap-fah)] (**8**)	MeOH	395 (2.3×10^3), 328 (3.4×10^4), 243 (3.7×10^4), 203 (4.6×10^4)
[$V^{V}O_2$ (Hap-nah)] (**9**)	MeOH	401 (2.3×10^3), 333 (5.1×10^4), 244 (4.3×10^4), 203 (2.6×10^4)
[$V^{V}O_2$ (Hap-inh)] (**10**)	MeOH	389 (1.8×10^3), 338 (2.1×10^4), 243 (2.9×10^4), 205 (3.6×10^4)
[V^{V}O(ap-bhz)(OMe)(MeOH)] (**11**)	MeOH	402 (2.6×10^3), 370 (3.1×10^4), 242 (2.6×10^4), 205 (3.3×10^4)
[V^{V}O(ap-fah)(OMe)(MeOH)] (**12**)	MeOH	401 (1.9×10^3), 367 (2.8×10^4), 238 (2.9×10^4), 203 (3.3×10^4)
[V^{V}O(ap-nah)(OMe)(MeOH)] (**13**)	MeOH	395 (1.4×10^3), 356 (2.2×10^4), 237 (3.3×10^4), 204 (4.1×10^4)
[V^{V}O(ap-inh)(OMe)(MeOH)] (**14**)	MeOH	391 (2.4×10^3), 346 (3.1×10^4), 241 (3.2×10^4), 201 (2.9×10^4)

^{1}H NMR Spectral Studies

^{1}H NMR spectra of ligands **I**–**IV** and their $V^{V}O/V^{V}O_2$ complexes were recorded to characterize them and confirm the coordination modes. The relevant data are presented in Table S3 (Supporting Information) and representative spectra {H_2ap-fah (**II**), $K(H_2O)_{0.5}[V^{V}O_2$(ap-fah)](**6**) and [$V^{V}O_2$ (Hap-fah)] (**8**)} are presented in Figure 8. Signals appearing at δ = 11.27–11.50 ppm in the ligand spectra, due to the NH proton, and at δ = 2.33–2.35 ppm, due to the ring proton of pyrazole residue, indicate the ketonic form of both C=O groups. The absence of these signals in spectra for complexes **5**, **6**, **11**–**14**, suggests the enolization and subsequent coordination of both oxygen atoms. Neutral complexes, **7** and **8**, show this signal at nearly the same position, possibly due to protonation of the hydrazido nitrogen (see the description of the crystal structure) and the presence of the C=O group in the ketonic form. In complexes **9** and **10**, although neutral, such resonance could not be located. Therefore, charge neutralization is probably accomplished by protonation of the pyridinic N atom. Coordinated methanol/methoxide (in complexes **11**–**14**) exhibits signals due to methyl and alcoholic protons at δ = 3.15–3.16 and 4.12–4.13 ppm, respectively. Aromatic protons appear in the expected region for both the ligands and complexes with slight shifts in their positions. All spectra the ligands display two signals at 2.36–2.37 and 2.40–2.46 ppm, due to methyl protons present on the pyrazole ring and on the azomethine nitrogen, respectively. The later signal shifts downfield due to N-atom and metal centre coordination. Thus, ^{1}H NMR spectroscopic data complement the conclusions drawn from IR data.

^{13}C NMR Spectral Studies

The coordination modes of the ligands towards the metal centre were further corroborated by ^{13}C NMR chemical shifts study. Table S4 presents ^{13}C NMR spectroscopic data of ligands and complexes and ^{13}C NMR spectra of H_2ap-fah (**II**), $K(H_2O)_{0.5}[V^{V}O_2$(ap-fah)] (**6**) and [$V^{V}O_2$(Hap-fah)] (**8**) are depicted in Figure 9. Ligands **I**, **II**, **III** and **IV** exhibit 15, 14, 15 and 15 ^{13}C NMR signals against a total of 19, 18, 18 and 17 carbon atoms, respectively. When compared to the ligand spectra, the corresponding metal complex spectra exhibit normally the same or a higher number of signals. A downfield coordination-induced shift, $\Delta\delta$ = [δ(complex) – δ(ligand)] is observed in the signals of the carbon atoms i.e. C1, C4 and C13, present in the vicinity of the coordinating atoms O, N and O [i.e. pyrazolone oxygen, azomethine nitrogen and enolic oxygen], respectively, confirming the coordination of these functionalities to the vanadium centre. The peaks due to other carbon atoms i.e. due to the phenyl ring, methyl group and pyrazole ring appear at the expected δ values in the spectra of ligands as well as in the complexes, with slight variations. In addition, two new signals appear in the spectra of **11**–**14** at 52.5–54.5 ppm and 61.3–62.9 ppm. These signals correspond to coordinated methanol and methoxy carbon atoms, respectively.

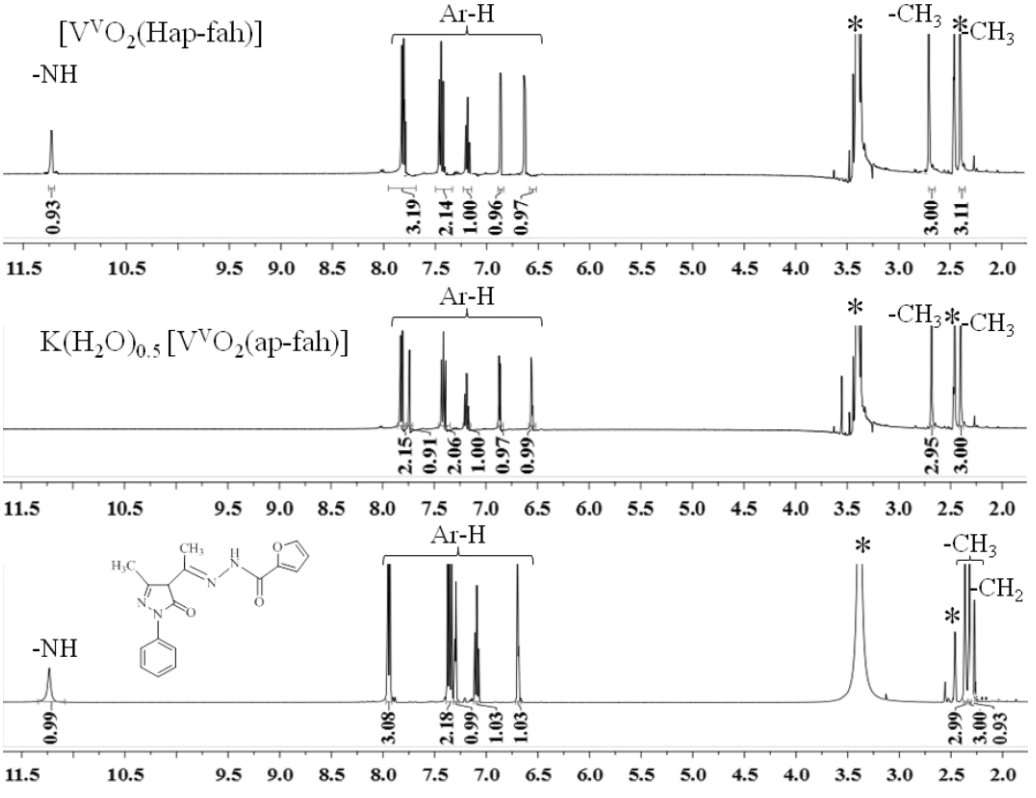

Figure 8. ^{1}H NMR spectra of H_2ap-fah (**II**), $K(H_2O)_{0.5}$ [$V^{V}O_2$(ap-fah) (**6**)] and [$V^{V}O_2$(Hap-fah)] (**8**) recorded in [D_6]DMSO. Star in Figure indicates signal due to water in DMSO/DMSO itself.

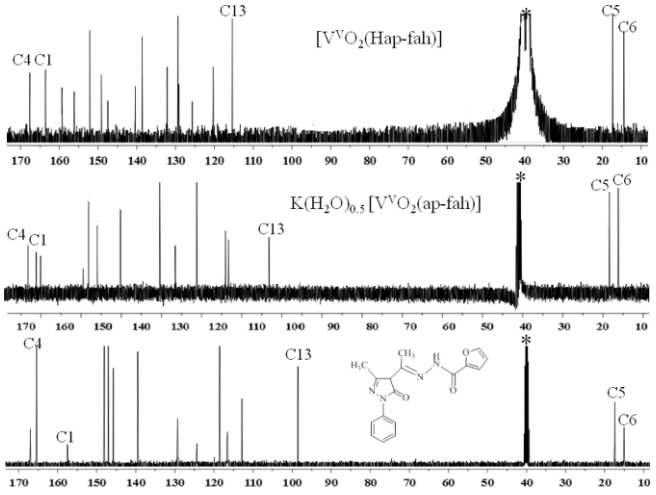

Figure 9. ^{13}C NMR spectra of H_2ap-fah (**II**), $K(H_2O)_{0.5}[V^VO_2$(ap-fah)] (**6**) and $[V^VO_2$(Hap-fah)] (**8**) recorded in [D_6]DMSO. The star in the figure denotes the carbon signals for DMSO.

^{51}V NMR Spectral Studies

Further characterization of the complexes was ascertained from ^{51}V NMR spectra. Table 4 contains the chemical shift values obtained for each complex dissolved in either DMSO or MeOH, before and after the addition of aqueous H_2O_2. The chemical shift values for $V^{IV}O$ complexes **1**–**4** were measured in solutions that were left under an atmosphere of air for 3 d and therefore correspond to oxidized species (+5). The δ values vary between –508.5 ppm (complex **3**) and –512.4 ppm (complex **2**) and are roughly the same as the ones found for corresponding V^VO_2 complexes **5**–**10**, which vary between –506.2 (complex **9**) and –512 ppm (complex **5**). The chemical shift values are within the usual range for tridentate ONO ligands.[23] We can therefore conclude that aerial oxidation of the $V^{IV}O$ complexes leads to the formation of corresponding V^VO_2 complexes. For **1** and **2** a lower field peak is present, corresponding either to an isomer, or a solvolysis product.

For V^VO complexes **11**, **12** and **14**, the spectra measured in MeOH show one sharp peak between –490.4 and –497.9 ppm. Typically, methoxy containing species resonate in this down-field region, since methanol and/or methoxy coordination increases the metal shielding, shifting the resonance to less negative values.[24] Complex **13** shows a much broader resonance at –515.5 ppm, which is also present in the NMR spectrum of **14**, but is much less important. These resonances are tentatively attributable to loss of the MeOH molecule.

Electrochemical Studies

The electrochemical behavior of the ligands and complexes was investigated by cyclic voltammetry and differential pulse voltammetry (DPV); and the CV results are given in Table S5 (Supporting Information). As a representative example, the cyclic voltammograms of ligand **I**, and respective complexes **1**, **7** and **11**, are displayed in Figure 10. The oxidation and reduction potentials in complexes **1**–**14** are within the range reported for similar compounds in the literature.[25]

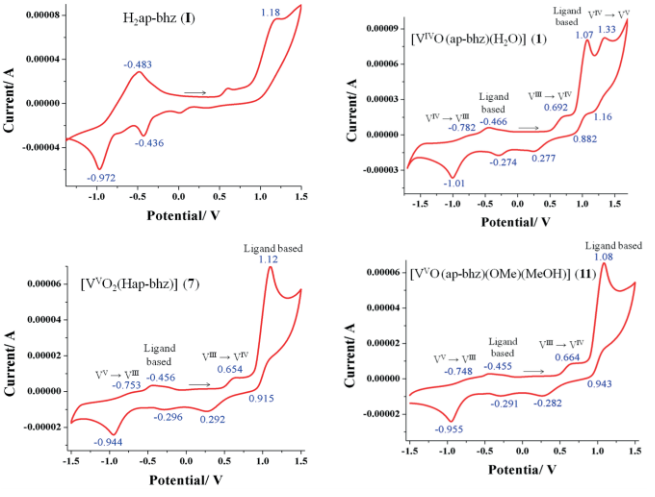

Figure 10. Cyclic voltammograms of ligand **I** and respective complexes in DMF vs. SCE. Conditions: ca. 1.0 mM metal complex concentration, 0.1 M Bu_4NPF_6, Pt disk working electrode, scan rate 0.1 V/s.

The ligand voltammogram in the potential range –1.5 to 1.5 V exhibit one peak at ca. +1.0 V due to ligand oxidation (hydrazine-based oxidation).[26] It also exhibits a reduction peak

Table 4. ^{51}V NMR spectroscopic data of the complexes dissolved in DMSO with 5 % D_2O, with and without H_2O_2 (final concentration indicated); [complex] ≈ 3 mM.

	δ [%]	δ [%] after addition of H_2O_2	[H_2O_2] [mM]
1[a]	–480.0 (20); –509.9 (80)	–513.3 (63); –615.8 (12.5); –634.0 (24.5)	360
2[a]	–474.4 (20); –512.4 (80)		
3[a]	–508.5 (100)		
4[a]	–509.7 (100)		
5	–512.4 (100)	–514.0 (80); –632.0 (10); –646.7 (10)	95
6	–511.7 (100)	–519.9 (95); –646.1 (2.5); –660.0 (2.5)	280
7	–476.2 (5); –508.2 (95)	–513.9 (80); –619.9 (10); –637.9 (10)	260
8	–510.9 (100)	–516.0 (80); –631.0 (10); –646.0 (10)	237
9	–506.2 (100)	–511.0 (15); –537.2 (70); –636.1 (7.5); –649.0 (7.5)	260
10	–509.0 (100)	–547.0 (95); –640.8 (2.5); –653.0 (2.5)	226
11[b][c]	–490.4 (100)	–555.7 (43); –660.1 (28.5); –679.8 (28.5)	173
12[b]	–497.9 (100)	–551.0 (43); –656.5 (28.5); –675.2 (28.5)	163
13[b][c]	–515.5 (100)	–516.0 (48); –639.1 (26); –654.0 (26)	73
14[b][c]	–491.6 (90); –514.8 (10)	–581.9 (80); –656.3 (20)	150

[a] The chemical shift values are from the species originating from aerial oxidation of the $V^{IV}O$ complexes. [b] In MeOH. [c] Precipitation occurred.

at –0.483 to –0.528 V, equivalent to two electrons, which is coupled with two closely associated peaks at –0.404 to –0.436 V and –0.889 to –0.972 V, attributed to the reduction of –N=CH– linkage of the ligand.[27] The peak potentials are shifted (ca. 100–200 mV) and the intensity of some signals are found to decrease in the corresponding CVs of the vanadium complexes due to incorporation of the metal centre. Therefore, the voltammograms of the metal complexes show both metal-based and ligand-based redox process.

The dioxidovanadium(V) complex exhibits a weak reduction peak (irreversible) at ca. –0.753 V due to the change $V^{V} \rightarrow V^{III}$ and another weak peak at ca. +0.55 V due to $V^{III} \rightarrow V^{IV}$.[28,29] The absence of any redox couple due to V^{IV}/V^{V} indicates that the complex is quite stable in the +5 oxidation state and also less susceptible towards oxidation or reduction processes in DMF.

The monoxidovanadium(IV) complex **1** exhibits a reduction peak at –0.782 V, due to the $V^{IV} \rightarrow V^{III}$ couple.[30] A quasi-reversible peak at ca. 1.33 V, as well as the associated coupled peak at 1.16 V, are due to a $V^{IV} \rightarrow V^{V}$ conversion.[31] No reduction process assignable to $V^{III} \rightarrow V^{II}$ was observed in any voltammogram. The electrochemical properties of all vanadium(IV) complexes, **1**–**4**, are similar and they display identical redox processes, confirming similar structures and electronic features. All these redox processes were supported by DPV (see Table 9).

EPR Characterization

The $V^{IV}O$ complexes were further characterized by EPR. The spectra of frozen solutions (at 77 K) of the $V^{IV}O$ – complexes exhibit a hyperfine pattern consistent with axial-type spectra of monomeric $V^{IV}O$-bound species with d^{1}_{xy} ground-state configurations. Figure S7 (Supporting Information) shows the X band EPR spectra measured for 3 mM solutions of the compounds in DMSO. The spectra are very similar for all complexes and their simulation[32] yielded similar spin-Hamiltonian parameters for complexes **1** and **2** and for **3** and **4**, which are included in Table 5. Once a particular binding mode is assumed, the values of $A_{||}$ can be estimated (A_{est}) using the additivity relationship proposed by Würthrich[33] and Chasteen[34] with an estimated accuracy of $\pm 3 \times 10^{-4}$ cm^{-1}. In this work we will use the following contributions, for reasons presented elsewhere,[35] which assume that CO contributes as an O-enolate(–1), using the average value for N_{imine} (41.6×10^{-4} cm^{-1})[17c,23a] and 45.65×10^{-4} cm^{-1} for the water molecule contribution. This yields an A_{est} value of 162.5×10^{-4} cm^{-1}, lower than experimental values found for the $A_{||}$. The $A_{||}$ contribution of the CO group is probably higher than 37.6×10^{-4} cm^{-1} since this donor atom is not a typical O-enolate(–1) donor. Therefore, this A_{est} value is probably an underestimate. The differences found in the spin Hamiltonian parameters for complexes **1** and **2** and for **3** and **4**, are attributed to different electronic contributions imposed by the R substituents that probably make the O-enolate in **3** and **4** a better donor group.

Table 5. Spin Hamiltonian parameters obtained by simulation of the EPR spectra with the computer program disclosed by Rockenbauer and Korecz.[32]

Complex	$g_{\perp}$	$g_{||}$	$A_{\perp}/\times 10^{4}$ cm^{-1}	$A_{||}/\times 10^{4}$ cm^{-1}
1	1.983	1.942	65.6	177.9
2	1.983	1.943	65.6	177.3
3	1.984	1.956	58.8	166.6
4	1.984	1.955	60.0	167.7

Reactivity of Oxidovanadium (IV) Complexes towards H_2O_2

The reactivity of oxidovanadium(IV) and dioxidovanadium(V) complexes towards H_2O_2 was monitored by UV/Vis absorption spectroscopy, with complex **1** serving as a representative of $[V^{IV}OL(H_2O)]$ complexes (Figure 11). The progressive addition of H_2O_2 to a solution of **1** in DMSO causes changes in the ligand centred, as well as metal centred d–d bands. These changes include flattening of the band at 345 nm, along with a shift of the band at 217 nm to 247 nm and flattening of the d–d band appearing at 636 nm, which finally disappears, indicating oxidation of the oxidovanadium(IV) complex to a higher oxidation state. Changes observed for complex **2** are reported in Figure S8 (Supporting Information) and include the disappearance of the d–d band.

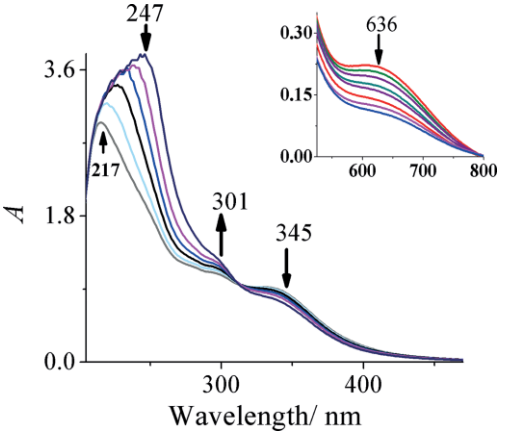

Figure 11. Spectral changes observed during titration of $[V^{IV}O(ap\text{-}bhz)(H_2O)]$ (**1**) with H_2O_2. The spectra were recorded following stepwise additions of one drop portions of 1.56×10^{-2} M of H_2O_2 solution to 25 mL of a 2.32×10^{-4} M solution of complex **1** in DMSO over the course of ca. 20 min. The inset shows changes observed during the titration of **1** with H_2O_2 for the d–d band of this complex. These spectra were recorded following stepwise additions of one drop portions of 1.35×10^{-2} M of H_2O_2 to 25 mL of 1.54×10^{-3} M solution of complex **1** in DMSO.

The process was also studied by ^{51}V NMR spectroscopy. Addition of aliquots of H_2O_2 (1 M) to 3 mM solutions containing complex **1** dissolved in DMSO, revealed oxidation of the $V^{IV}O$ complex, with a peak appearing at –510 ppm (as well as a smaller one at ca. –480 ppm, see Figure S9, Supporting Information). Following the addition of a large excess of H_2O_2 (120 mM), peaks assigned to mono- and di-peroxovanadate species appeared upfield. Addition of H_2O_2 increased the linewidth and it is possible that more than one species was present under the resonance peak; consequently, we cannot exclude the formation of $[V^{V}O(O_2)L]$ species.

Reactivity of Dioxidovanadium(V) Complexes

The reactivity of dioxido complexes towards H_2O_2 was evaluated with the same spectroscopic tools. Changes were ob-

served in the UV/Vis spectra, namely isosbestic points, confirming the formation of new species. Using complex **5** as a representative, the spectra measured during its titration in MeOH with H_2O_2 are shown in Figure 12. Spectral changes for the other complexes are included in Figures S10–S12 (Supporting Information).

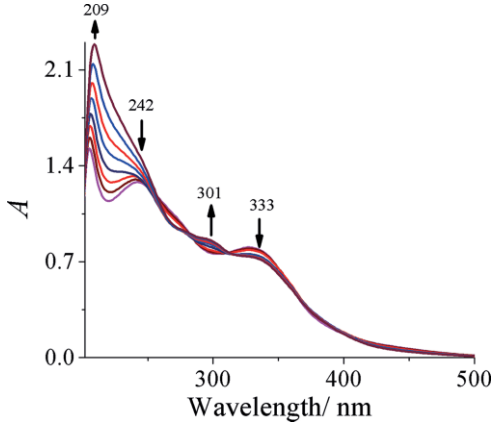

Figure 12. Spectral changes observed during titration of complex **5** with H_2O_2. The spectra were recorded following stepwise additions of one drop portions of 2.38×10^{-2} M H_2O_2 solution of **5** to 25 mL of 3.45×10^{-4} M solution in MeOH over the course of ca. 20 min.

The reactivity of V^VO_2 complexes **5**–**10** towards H_2O_2 was evaluated using ^{51}V NMR spectroscopy. Spectra for all the characterized systems are included in Figures S13–S17 (Supporting Information); Table 4 also lists the chemical shifts of the resonances observed in the spectra with the higher H_2O_2 concentration (also included in the Table). For complexes **5**–**8** the linewidth of the resonance assigned to the V^VO_2 complex increases with the addition of H_2O_2 and a small upfield shift is observed (<10 ppm). At some point, peaks assigned to $V^VO(O_2)^+$ and $V^VO(O_2)_2^-$ appear and shift upfield commensurate with increased H_2O_2 concentration. However, for complexes **9** and **10** (see Figure 13 for complex **10**) it is very interesting to observe that what seems to be one resonance becomes two separate

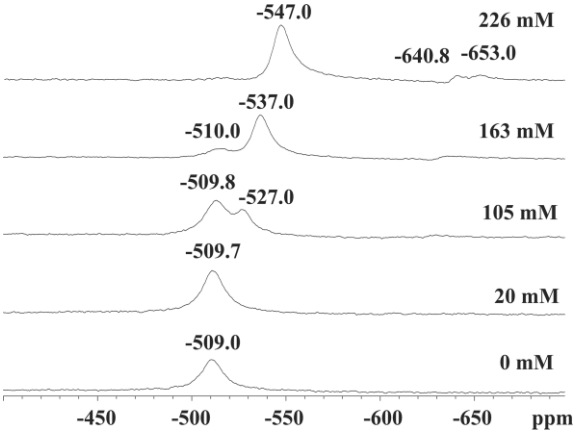

Figure 13. ^{51}V NMR spectra measured for a solution containing complex **10** (3 mM) dissolved in DMSO with 5 % D_2O, after addition of H_2O_2 1 M. Concentration of H_2O_2 indicated in the Figure.

ones, with the up field signal increasing in intensity and the downfield signal decreasing as more H_2O_2 is added. The upfield peak is assigned to $V^VO(O_2)L$ since the presence of the peroxide molecule in the coordination sphere increases the electron density and therefore shields the vanadium centre. We can also assume that the linewidth broadening observed in the resonances of complexes **5**–**8** with increasing H_2O_2 concentration is also due to the presence of more than one complex species, one of them being the peroxido complex $V^VO(O_2)L$.

Reactivity of Monooxidovanadium(V) Complexes

^{51}V NMR was also used to study the reactivity of the $[V^VOL(OMe)(MeOH)]$-type complexes **11**–**14**. Figure 14 shows the spectra measured for complex **11** before and after addition of increasing concentrations of H_2O_2 and others are included as Supporting Information. In MeOH, the line widths are much lower than observed in DMSO and a peak at ca. –550 ppm [for **11** (Figure 14) and 1**2** (Figure S18, Supporting Information)] or –580 ppm (for **13** and **14**, see Figures S19 and S20, Supporting Information) appears and grows at the expense of the $V^VOL(OMe)(MeOH)$ peak. We assign this peak as $V^VO(O_2)L^-$, $V^VO(O_2)L(OMe)^{2-}$ or $V^VO(O_2)L(OMe)(MeOH)^{2-}$-type complexes. Since the chemical shift is similar to that found for complex **10** in DMSO, we propose the absence of coordinated MeO^- or MeOH molecules. Free-ligand inorganic peroxovanadate species also appear further upfield in all systems at ca. 650–680 ppm. Complex **13** seems less prone to forming the peroxido species, since only a very small amount is present at 73 mM of H_2O_2.

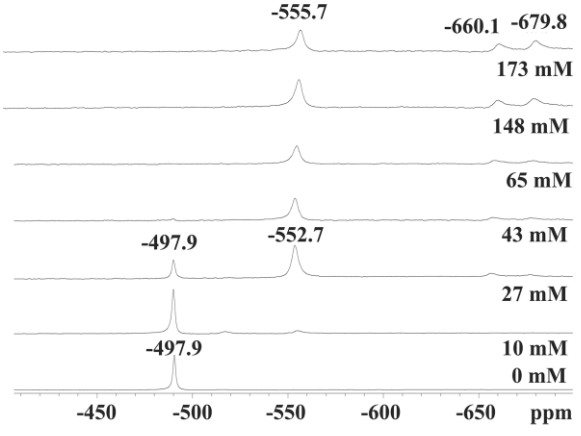

Figure 14. ^{51}V NMR spectra measured for a solution of complex **11** (ca. 3 mM) dissolved in MeOH containing 5 % D_2O, before and after addition of H_2O_2 (1 M). Concentration of H_2O_2 indicated in the Figure.

Reactivity of Dioxidovanadium (V) Complexes with HCl

The behaviour of a methanolic solution of complex **6** upon titration with HCl was also studied spectrophotometrically. Complex **6** (ca. 10^{-4} M solution in methanol) was treated with one drop portions of methanol saturated with HCl gas; the observed changes are presented in Figure 15. These results possibly re-

flect the formation of dioxido vanadium species with one of the N–N nitrogen atoms being the site of protonation upon acidification.

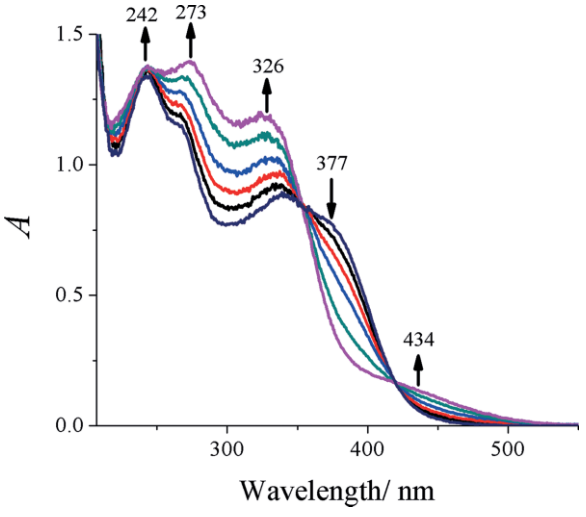

Figure 15. Spectral changes observed during titration of complex **6** with methanolic HCl solution. The spectra were recorded upon stepwise additions of one drop portions of HCl solution (1.3×10^{-1} M) in MeOH to 25 mL of 4.3×10^{-4} M solution of complex **6** in MeOH during ca. 20 min.

Peroxidase Mimetic Activity towards the Oxidation of Pyragallol

The peroxidase mimetic activity of [V^{V}O(ap-fah)(OMe)(MeOH)] (**12**) was investigated towards the oxidation of pyrogallol in the presence of H_2O_2 as an oxidant. This reaction yields purpurogallin (Scheme 3) whose formation can be monitored by UV/Visible spectroscopy. In the presence of H_2O_2, the pyrogallol solution turns yellow with a very weak absorption at ca. 420 nm due to the formation of purpurogallin,[36] which is absent in pyrogallol.

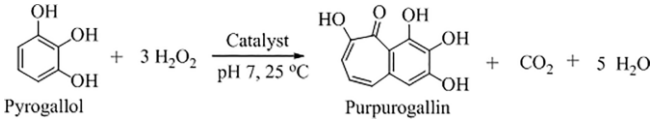

Scheme 3. Catalytic oxidation of pyrogallol to purpurogallin.

The following sets of samples were prepared and the resulting spectral changes were followed by UV-spectrophotometry after 5 min of their preparation: i) pyrogallol in MeCN/phosphate buffer (pH 7, 1 M); ii) same solution after addition of 1 mL of 0.025 M H_2O_2 and iii) after addition of 1.0 $\times 10^{-3}$ g (2.2×10^{-6} mol) catalyst **12**.

The formation of purpurogallin was confirmed by the appearance of a weak band at ca. 420 nm, after addition of H_2O_2. However, in the presence of catalyst, this characteristic absorption band becomes much sharper and intense (Figure S21, Supporting Information) following the conventional enzymatic dynamic regulation of the Michaelis–Menten equation. Figure 16 shows changes observed with time and suggests that the reaction reaches maximum measurable absorbance within 1 h.

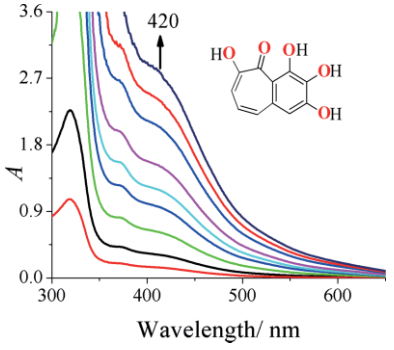

Figure 16. Electronic absorption spectra due to the formation of purpurogallin over time. Reaction conditions: pyrogallol solution 1 mL (0.025 M) mixed with 3 mL phosphate buffer (pH 7, 1 M), 1 mL of 30 % H_2O_2 (0.025 M) and 3.0 $\times 10^{-3}$ g (6.6×10^{-6} mol) catalyst, 1 h of reaction time at 25 °C.

In order to optimize the reaction conditions for optimal oxidation of pyrogallol, several parameters, such as different amounts of catalyst and oxidant were varied. Five different concentrations of catalyst (i.e. from 1.0×10^{-3} to 5.0×10^{-3} g) were tested using a fixed amount of pyrogallol (1 mL of 2.5×10^{-2} M in MeCN) in 3 mL of 1 M pH 7 phosphate buffer; 1 mL of 2.5×10^{-2} M solution of H_2O_2 and 25 °C reaction temperature. The oxidation of pyragallol was greatly facilitated by increasing the catalyst amount from 1.0×10^{-3} g (2.2×10^{-6} mol) to 2.0×10^{-3} g (4.4×10^{-6} mol) (Figure 17). Only a small improvement in pyragallol oxidation was noted when 3.0×10^{-3} g (6.6×10^{-6} mol) of catalyst was applied whereas further increments in catalyst rendered little change to the rate of oxidative conversion. Consequently, a 3.0 $\times 10^{-3}$ g (6.6×10^{-6} mol) of catalyst per reaction was deemed ideal for subsequent efforts to optimize other reaction conditions.

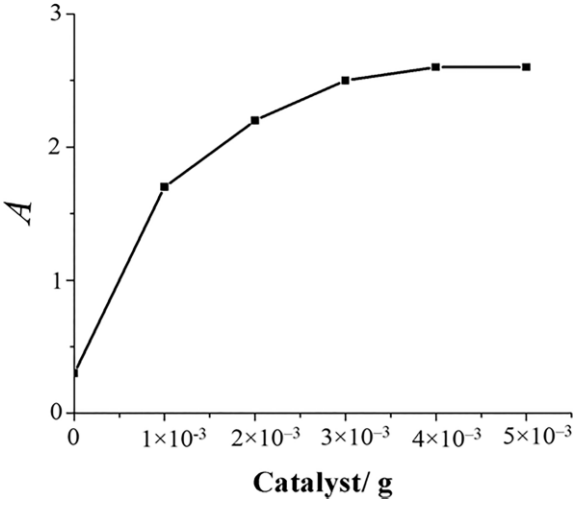

Figure 17. Plot of absorbance at 420 nm after 1 h of reaction time for peroxidase-like activity using pyrogallol at different catalyst amounts. Other reaction conditions: pyrogallol solution (prepared in MeCN) (1 mL of 2.5×10^{-2} M), phosphate buffer solution (3 mL, pH 7, 1 M), 30 % H_2O_2 (1 mL of 2.5×10^{-2} M) and reaction temperature (25 °C).

The effect of oxidant concentrations (i.e. H_2O_2) in the oxidation of pyrogallol was then studied by examining reactions with five different oxidant concentrations. Thus, 1 mL of H_2O_2

solution with different concentrations (2.5×10^{-2}–2.5×10^{-6} M) was added to each sample containing a fixed amount of pyrogallol [1 mL of 2.5×10^{-2} M in MeCN and pH 7 phosphate buffer (3 mL of 1 M)], and catalyst **12** (3×10^{-3} g, 6.6×10^{-6} mol). The reaction was monitored at 25 °C for 1 h and Figure 18 presents the absorbance at λ_{max} = 420 nm at different concentrations of H_2O_2. The catalyst shows a very good response to different H_2O_2 concentrations, with the formation of purpurogallin doubling when going from 2.5×10^{-6} to 2.5×10^{-5} M oxidant. The use of 2.5×10^{-4} M H_2O_2 yielded reasonably good activity at very low concentrations of H_2O_2 under the above optimized reaction conditions.

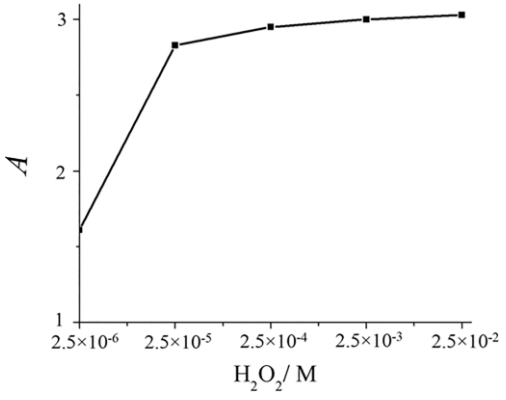

Figure 18. Plot of absorbance at 420 nm after 1 h of reaction time for peroxidase-like activity using pyrogallol at different concentrations of H_2O_2. Other reaction conditions: pyrogallol solution (prepared in MeCN) (1 mL of 2.5×10^{-2} M), phosphate buffer solution (3 mL of pH 7, 1 M), catalyst **12** (3.0×10^{-3} g, 6.6×10^{-6} mol) and reaction temperature (25 °C).

To further explore the peroxidase mimetic activity of **12**, kinetic parameters such as V_{max}, K_M, k_{cat} (where V_{max} is the maximum rate, K_M is the Michaelis–Menten constant and k_{cat} is the turnover number) were determined. Several experiments were conducted at 25 °C by varying the concentration of pyrogallol from 0.20 mM to 2.6 mM under the optimized reaction conditions {i.e. pH 7 phosphate buffer solution (3 mL of 1 M), catalyst [V^{V}O(ap-fah)(OMe)(MeOH)] (3.0×10^{-3} g, 6.6×10^{-6} mol) and 30 % H_2O_2 (1 mL of 2.5×10^{-4} M)}. Experiments were run in triplicate and the initial reaction rates were calculated by measuring the absorbances at 420 nm and taking the triplicate average after carrying out each reaction for 5 min.

Typically, the rate of enzyme–mimetic reactions does not show a linear response with increasing substrate concentration. However, if the initial rate of the reaction is measured over a range of substrate concentrations, the reaction rate (v) increases as [S] increases. As [S] increases, the enzyme becomes saturated with substrate and the rate reaches V_{max}, the enzyme's maximum rate. This phenomenon can be explained by the Michaelis–Menten equation [Equation (6)], where V_i is the initial reaction rate, V_{max} is the maximum rate, [*S*] is the concentration of substrate and K_M is the Michaelis–Menten constant.

$$V_i = V_{max} \times \frac{[S]}{K_M + [S]} \quad (6)$$

For catalyst **12**, V_i follows saturation kinetics with respect to [*S*]. The rate of reaction is first-order at low substrate concentrations [*S*] (i.e. a linear plot is obtained for V_i vs. [*S*]). At sufficiently high [*S*] the catalyst becomes saturated with the substrate and the rate of reaction is zero-order. The kinetic parameters, Michaelis binding constant (K_M) and V_{max} were obtained from analysis of the experimental data and the turnover number (k_{cat}) value is obtained from dividing the V_{max} by the concentration of the complex used [Equation (7)]. Thus, complex **12** clearly displays Michaelis–Menten behaviour towards pyrogallol; the Lineweaver–Burk plot is shown in Figure 19. The V_{max} obtained was 2.1 μM min^{-1} and the turnover number (k_{cat}) was 7.1 min^{-1} for catalyst **12** as dictated by [Equation (7)].

$$K_{cat} = \frac{V_{max}}{\text{concentration of enzyme}} \quad (7)$$

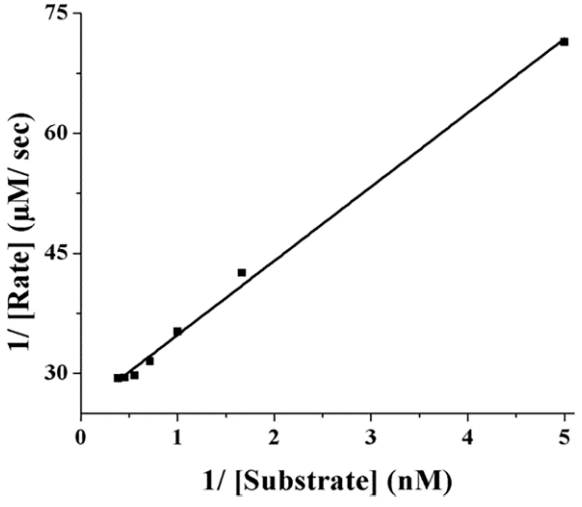

Figure 19. Lineweaver–Burk linearization plot for pyrogallol over the concentration range (0.20–2.2 mM). The concentration of H_2O_2 and **12** remain constant in phosphate buffer (pH 7, 1 M).

Oxidomethoxidovanadium(V) complexes **11**, **13** and **14** were also tested in the oxidation of pyrogallol; Table 6 summarizes the results. Notably, all catalysts showed similar behaviours with comparable V_{max} and k_{cat} values (see Figure S22, Supporting Information) relative to the reactions with catalyst **12**.

Table 6. Kinetic parameters for peroxidise activity of complexes **11**–**14**.

	Complex/catalyst	V_{max}/ [μM/min^{-1}]	TOF (k_{cat}) [min^{-1}]
1	[V^{V}O(ap-bhz)(OMe)(MeOH)] (**11**)	2.7	8.2
2	[V^{V}O(ap-fah)(OMe)(MeOH)] (**12**)	2.2	7.1
3	[V^{V}O(ap-nah)(OMe)(MeOH)] (**13**)	2.6	8.0
4	[V^{V}O(ap-inh)(OMe)(MeOH)] (**14**)	2.5	7.7

Thus, from the calculated k_{cat} and V_{max} values it can be concluded that the complexes herein synthesized are, indeed, functional models of artificial peroxidases, showing peroxidase mimetic activity. The catalytic potentials of the catalysts considered here are superior to those previously reported by us for the same oxidation reaction [K_{cat} (min^{-1}) = 4.79×10^{-3} for PS-[V^{V}O(OMe)(hap-iah)] (H_2hap-iah = Schiff base derived from 2-hydroxyacetophenone and indole-3-acetic acid hydrazide) and

K_{cat} (min^{-1}) = 3.62×10^{-3} for PS-$V^{IV}O$(Hsal-dahp)(DMSO)] (H_2sal-dahp = Schiff base derived from salicylaldehyde and 1,3-diamino-2-hydroxypropane).[16]

Catalytic Activity: Oxidation of 1-Phenylethanol

The selective catalytic oxidation of 1-phenylethanol to acetophenone (Scheme 4) also was evaluated using complexes **11**–**14** in the presence of H_2O_2.

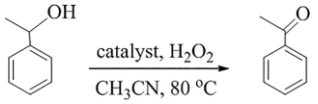

Scheme 4. Catalytic oxidation of 1-phenylethanol to acetophenone.

Complex **12** was selected as a representative catalyst precursor and efforts to optimize catalyst and oxidant amounts, solvent and temperature were undertaken. Thus, for 0.010 mol (1.2 g) of 1-phenylethanol, three different amounts of complex **12** (i.e. 1×10^{-3}, 2×10^{-3} and 3×10^{-3} g); three concentrations of aqueous 30 % H_2O_2 (i.e. 0.010, 0.020 and 0.030 mol), in three different volumes of MeCN (5, 7 and 10 mL) were applied to establishing a library of reactions and these reactions were carried out at three different temperatures (60, 70 and 80 °C). Table 7 and Figure S23 (Supporting Information) present the details of the applied experimental conditions as well as ensuing conversion efficiencies. From Table 7 it is clear that increased catalyst or oxidant concentrations correlated to slightly improved conversions (Table 7, Entries 1–3, 4 and 5). Also evident is that reaction temperature has a strong effect (Table 7, Entries 7–9) and that the reaction conditions best suited for optimum conversion (i.e. 74 % with a turnover frequency of 576 h^{-1}) are (Table 7, Entry 2): catalyst (2×10^{-3} g, 4.4×10^{-6} mol), 30 % H_2O_2 (2.2 g, 0.020 mol), MeCN (5 mL) and a reaction temperature of 80 °C.

Table 7. Oxidation of 1-phenylethanol (1.2 g, 0.010 mol) under different reaction conditions using **12** as catalyst precursor.

Entry	H_2O_2 g [mol]	Catalyst g [μmol]	MeCN [mL]	Temp. [°C]	Conv. [%]	TOF [h^{-1}]
1	2.3 (0.020)	1×10^{-3} (2.2)	5	80	74	560
2	2.3 (0.020)	2×10^{-3} (4.4)	5	80	76	576
3	2.3 (0.020)	3×10^{-3} (6.6)	5	80	80	606
4	1.1 (0.001)	1×10^{-3} (2.2)	5	80	60	454
5	3.3 (0.030)	1×10^{-3} (2.2)	5	80	82	621
6	2.3 (0.020)	1×10^{-3} (2.2)	7	80	81	613
7	2.3 (0.020)	1×10^{-3} (2.2)	10	80	77	583
8	2.3 (0.020)	1×10^{-3} (2.2)	5	60	52	394
9	2.3(0.020)	1×10^{-3} (2.2)	10	70	67	507
10	2.3 (0.020)	–	5	80	32	

We have tested the catalytic potential of oxidomethoxidovanadium(V) complexes **11**, **13** and **14** in the oxidation of 1-phenylethnol under the optimized reaction conditions identified for complex **12**; Table 8 summarizes the results. All catalysts showed similar behaviours giving rise to conversion values within 80–85 %. A blank reaction, devoid of catalyst, under these conditions afforded a conversion value of only 32 %. Thus, the oxidation of 1-phenylethanol is clearly catalysed by the vanadium complexes evaluated.

Table 8. Oxidation of 1-phenylethanol using **11**–**14** under optimized reaction conditions (see Table 7, Entry 2).

	Complex	Substrate/ catalyst ratio	Conv. [%] (yield, mmol)	TOF [h^{-1}]
1	[VO(ap-bhz)(OMe)(MeOH)] (**11**)	$1{:}4.3 \times 10^{-4}$	86 (8.6)	651
2	[VO(ap-fah)(OMe)(MeOH)] (**12**)	$1{:}4.4 \times 10^{-4}$	76 (7.6)	576
3	[VO(ap-nah)(OMe)(MeOH)] (**13**)	$1{:}4.3 \times 10^{-4}$	81 (8.1)	613
4	[VVO(ap-inh)(OMe)(MeOH)] (**14**)	$1{:}4.3 \times 10^{-4}$	80 (8.0)	606

Based on these experiments (UV/Vis and ^{51}V NMR) the following reaction Scheme for both catalytic reactions is proposed (Scheme 5).

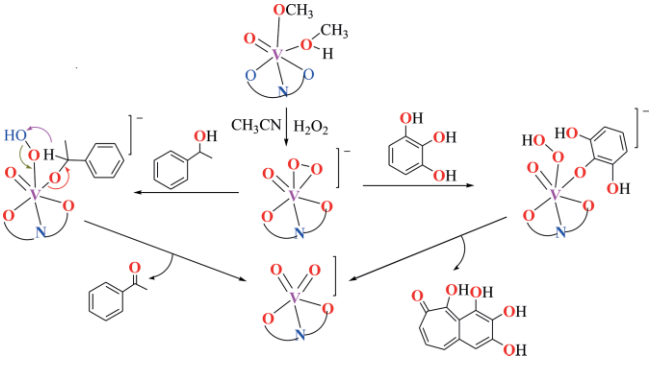

Scheme 5. Proposed reaction scheme for the catalytic reactions.

The catalytic oxidation of 1-phenylethanol by the catalysts reported here compares well with the catalytic potential of molybdenum-based catalysts [$Mo^{VI}O_2$(dha-inh)(MeOH)] (where H_2dha-inh = Schiff base derived from dehydroacetic acid and isonicotinoyl hydrazide) and [$Mo^{VI}O_2$(bp-bhz)(MeOH)] (H_2bp-bhz = benzoylpyrazolone and benzoyl hydrazide) reported recently where 78 and 84 % conversions, respectively, were obtained.[37,38] Notably, conversions with vanadium complexes [VO(Hhpic)$_2$] (where Hhpic = 3-hydroxypicolinic acid) (51 %),[39] [$V_2O_2Mo_2O_4${μ-(O_2)}(4,4′-*t*Bubpy){μ-($OMe)_2$}] (where 4,4′-*t*Bubpy = 4,4′-di-*tert*-butyl-2,2′-bipyridyl) (63 %), and [$V_2O_2W_2O_4${μ-(O_2)}(4,4′-*t*Bubpy){μ-($OMe)_2$}] (28 %)[40] are much lower than those achieved by the complexes reported here.

Conclusions

Vanadium complexes of general compositions [V^{IV}OL(H_2O)], K($H_2O)_n$[V^VO_2L] (n = 1 or 0.5), [V^VO_2(HL)] and [V^VO(L)(OMe)-(MeOH)] where L is a dianionic ONO ligand derived from acetylpyrazolone (ap) and different hydrazides – benzoyl hydrazide (bhz), 2-furoyl hydrazide (fah), nicotinoyl hydrazide (nah) and isonicotinoyl hydrazide (inh) have been successfully synthesized and characterized. The molecular structures of complexes K($H_2O)_{0.25}$[V^VO_2(ap-fah)] (**6**), [V^VO_2(Hap-bhz)]·H_2O (**7**), [V^VO_2(Hap-nah)] (**9**), [V^VO_2(Hap-inh)]·H_2O (**10**), [V^VO(ap-bhz)(OMe)(MeOH)] (**11**) and [V^VO(ap-fah)(OMe)(MeOH)] (**12**) were elucidated by single-crystal X-ray diffraction analyses. In complexes **7** and **8** protonation of the hydrazide nitrogen takes place; protonation in complexes **9** and **10** occurs at the pyridine

nitrogen. The complexes show excellent catalytic activity in the oxidation of 1-phenylethanol to give acetophenone. Thus, the synthesized complexes are structural and functional models of the vanadate-dependent haloperoxidases. The complexes were also successfully applied in the oxidation of pyrogallol to purpurogallin under mild reaction conditions in pH 7 buffered solution.

Experimental Section

Materials: Acetylacetone, furoyl hydrazide, pyrogallol, 1-phenylethanol (Aldrich Chemicals Co., U.S.A.), ethyl benzoate, hydrazine hydrate, isonicotinoyl hydrazide (Loba Chemie, Mumbai, India), nicotinoyl hydrazide (Acros organics, New Jersey, USA) and 30 % aqueous H_2O_2, (Rankem, New Delhi, India) were used as supplied. Other chemicals and solvents were of analytical reagent grade. $[V^{IV}O(acac)_2]$,[41] 3-methyl-1-phenyl-5-pyrazolone,[42] 4-acetyl-3-methyl-1-phenyl-2-pyrazoline-5-one[43] and ligands H_2ap-bhz (**I**), H_2ap-fah (**II**), H_2ap-nah (**III**) and H_2ap-inh (**IV**)[18] were prepared according to methods reported in the literature.

Instrumentation and Characterization Procedures: Elemental analysis (C, H and N) were carried out on an elementar model Vario-E1–III after drying the complexes in vacuo over silica gel for several hours. IR spectra were recorded as KBr pellets with a Nicolet 1100 FT-IR spectrometer. Electronic spectra of ligands and complexes were measured in methanol or in DMSO either with a Shimadzu 1601 or with a Perkin–Elmer lambda 35 UV/Vis spectrophotometer. ^1H and ^{13}C NMR spectra were recorded in $[D_6]$DMSO using a Bruker Advance 500 MHz. ^{51}V-NMR spectra of ca. 3 mM solutions of the complexes in DMSO or MeOH (p.a. grade) (5 % D_2O was added) were recorded with a Bruker Avance III 400 MHz instrument. ^{51}V chemical shifts were referenced relative to neat $VOCl_3$ as external standard. The following parameters were used: number of scans 2000–5000; line broadening 100 Hz; spectral resolution 12.7 Hz; spectral width 3959 ppm; acquisition time 0.039 s; FID resolution 25.4 Hz; receiver gain 203; dwell time 1.2 μs. The thermogravimetric analysis of the complexes was carried out under an oxygen atmosphere using a TG Stanton Redcroft STA 780 instrument. The redox properties of the ligands (**I**–**IV**) and the complexes (**1**–**14**) were studied by cyclic voltammetry and differential pulse voltammetry using CH Electrochemical workstations instruments with a three compartment cell provided with Pt as working electrode, platinum wire as counter electrode and standard calomel electrode (SCE) as reference electrode. Tetrabutyl ammonium phosphate (TBAP) was used as supporting electrolyte in DMF under an argon-saturated atmosphere in the potential range –1.5 to 1.5 V at room temperature. A Shimadzu 2010 plus gas-chromatograph fitted with an Rtx-1 capillary column (30 m × 0.25 mm × 0.25 μm) and FID detector was used to analyze the reaction products and their quantification was made based on the relative peak area of each product. The identity of the products was confirmed using a GC–MS model Perkin–Elmer, Clarus 500 and comparing the fragments of each product with the library available. EPR spectra were recorded at 77 K with a Bruker ESP 300E X-band spectrometer coupled to a Bruker ER041 X-band frequency meter (9.45 GHz). The complexes were dissolved at room temperature in DMSO p.a. grade, previously degassed by passing N_2 for 10 min, to obtain ca. 3 mM solutions. Spectra were measured at 77 K and simulated with a program developed by Rockenbauer and Korecz.[32]

Preparations

$[V^{IV}O(ap\text{-}bhz)(H_2O)]$ (1): The ligand H_2ap-bhz (0.34 g, 0.0010 mol) was dissolved in methanol (15 mL) and filtered. A solution of $[V^{IV}O(acac)_2]$ (0.26 g, 0.0010 mol) in methanol (15 mL) was added to the above solution with stirring. The reaction mixture was refluxed on a water bath for ca. 6 h. The obtained clear solution was reduced to 10 mL and kept in the refrigerator (ca. 10 °C) where a black solid slowly precipitated out. The solid was filtered, washed with methanol followed by petroleum ether (b.p. 60 °C) and dried in a desiccator over silica gel, yield: 0.32 g (77 %). $C_{19}H_{18}N_4O_4V$ (417.31): calcd. C 54.68, H 4.35, N 13.43; found C 54.7, H 4.3, N 13.4.

$[V^{IV}O(ap\text{-}fah)(H_2O)]$ (2): Complex **2** was prepared from the method outlined for complex **1** using H_2ap-fah, yield: 0.32 g (78 %). $C_{17}H_{16}N_4O_5V$ (407.27 g/mol): calcd. C 50.13, H 3.96, N 13.76; found C 50.4, H 3.8, N 14.0.

$[V^{IV}O(ap\text{-}nah)(H_2O)]$ (3): Complex **3** was prepared from the method outlined for complex **1** using H_2ap-nah, yield: 0.29 g (69 %). $C_{18}H_{17}N_5O_4V$ (418.30): calcd. C 51.68, H 4.10, N 16.74; found C 51.4, H 3.7, N 16.4.

$[V^{IV}O(ap\text{-}inh)(H_2O)]$ (4): Complex **4** was prepared from the method outlined for complex **1** using H_2ap-inh, yield: 0.30 g (72 %). $C_{18}H_{17}N_5O_4V$ (418.30): calcd. C 51.68, H 4.10, N 16.7; found C 51.8, H 4.2, N 16.6.

$K(H_2O)[V^{V}O_2(ap\text{-}bhz)]$ (5): V_2O_5 (0.18 g, 0.0010 mol) was suspended in an aqueous solution of KOH (0.11 g, 0.0020 mol in 5 mL of H_2O) and stirred for 2 h with occasional heating at 50 °C. The resulting clear solution was then filtered. A filtered solution of **I** (0.67 g, 0.0020 mol) dissolved in 50 mL of aqueous KOH (0.22 g, 0.0040 mol) was added to the above solution. The resulting mixture was allowed to react for 2 h and then the pH was adjusted to ca. 7.5 with 4 M HCl. The yellowish-orange solid started to separate within 30 min but the stirring was continued for the next 2 h. The separated solid was filtered, washed with cold water (2 × 5 mL) and dried in a desiccator over silica gel, yield: 0.30 g (67 %). $C_{19}H_{18}KN_4O_5V$ (472.27): calcd. C 48.31, H 3.84, N 11.86; found C 48.2, H 4.7, N 11.7.

$K(H_2O)_{0.5}[V^{V}O_2(ap\text{-}fah)]$ (6): Yellow complex **6** was prepared by the method described for complex **5** with **II** as ligand, yield: 0.33 g (72 %). $C_{17}H_{15}KN_4O_{5.5}V$ (453.30): calcd. C 45.00, H 3.31, N 12.35; found C 44.4, H 3.5, N 12.2.

$[V^{V}O_2(Hap\text{-}bhz)]$ (7): Complex **5** (0.45 g, 0.0010 mol) was dissolved in water (40 mL) and treated with dropwise addition of aqueous HCl (2 M) until most of the complex had precipitated as a yellow solid. After 1 h of stirring, the solution was filtered, the residue washed with water and dried in a desiccator over silica gel, yield: 0.24 g (57 %). $C_{19}H_{17}N_4O_4V$ (416.28): calcd. C 54.82, H 4.12, N 13.46; found C 55.8, H 4.4, N 14.0.

$[V^{V}O_2(Hap\text{-}fah)]$ (8): Complex **8** (yellow colour) was prepared from **6** following the method adopted for complex **7**, yield: 0.238 g (58.1 %). $C_{17}H_{15}N_4O_5V$ (406.28): calcd. C 50.26, H 3.72, N 13.79; found C 50.6, H 3.5, N 13.7.

$[V^{V}O_2(Hap\text{-}nah)]$ (9): V_2O_5 (0.18 g, 0.0010 mol) was suspended in an aqueous solution of KOH (0.11 g, 0.0020 mol in 5 mL of H_2O) and stirred for 2 h with occasional heating at 50 °C. The resulting clear solution was then filtered. A filtered solution of H_2ap-nah (**III**) (0.0020 mol) dissolved in aqueous KOH (50 mL, 0.22 g, 0.0040 mol) was added to the above solution with stirring. The resulting mixture was allowed to react for 4 h after which the pH of the reaction mixture was adjusted to ca. 7.0 with 4 M HCl, when yellowish-orange solid **9** started to separate. After 2 h of stirring the separated solid was filtered, washed with cold water (2 × 5 mL) and dried in a desiccator over silica gel, yield: 0.25 g (60.0 %). $C_{18}H_{16}N_5O_4V$ (417.30 g/mol): calcd. C 51.81, H 3.86, N 16.78; found C 51.7, H 3.5, N 17.0.

[$V^{V}O_2$(Hap-inh)] (10): Yellow complex **10** was prepared from ligand H_2ap-inh (**IV**) following the method described for **9**, yield: 0.25 g (61 %). $C_{18}H_{16}N_5O_4V$ (417.30 g/mol): calcd. C 51.81, H 3.86, N 16.78; found C 51.5, H 3.9, N 16.6.

[V^{V}O(ap-bhz)(OMe)(MeOH)] (11): Complex **1** (0.42 g, 0.0010 mol) was dissolved in MeOH (30 mL) and allowed to stand in the open flask for slow evaporation/oxidation. The dark solution slowly changed to orange-yellow from which a yellow solid separated within a week. The solid was filtered, washed with cold water and dried in a desiccator over silica gel, yield: 0.36 g (78 %). $C_{21}H_{23}N_4O_5V$ (462.37): calcd. C 54.55, H 5.01, N 12.12; found C 54.1, H 5.9, N 11.9.

[V^{V}O(ap-fah)(OMe)(MeOH)] (12): Complex **12** was prepared similarly to **11** from complex **2**, yield: 0.34 g (75 %). $C_{19}H_{21}N_4O_6V$ (452.33): calcd. C 50.45, H 4.68, N 12.39; found C 50.7, H 5.2, N 12.0.

[V^{V}O(ap-nah)(OMe)(MeOH)] (13): Complex **13** was prepared similarly to **11** from complex **3**, yield: 0.34 g (74 %). $C_{20}H_{22}N_5O_5V$ (463.36): calcd. C 51.84, H 4.79, N 15.11; found C 51.4, H 5.0, N 14.8.

Table 9. Crystal data and structure refinement for $\{K(H_2O)_{0.25}[V^{V}O_2(ap\text{-}fah)]\}_n$ (**6**), $[V^{V}O_2(Hap\text{-}bhz)]\cdot H_2O$ (**7**), $[V^{V}O_2(Hap\text{-}nah)]$ (**9**), $[V^{V}O_2(Hap\text{-}inh)]\cdot H_2O$ (**10**), $[V^{V}O(ap\text{-}bhz)(OMe)(MeOH)]$ (**11**) and for $[V^{V}O(ap\text{-}fah)(OMe)(MeOH)]$ (**12**).

	6	**7**	**9**
Formula	$C_{68}H_{56}K_4N_{16}O_{21}V_4$	$C_{19}H_{19}N_4O_5V$	$C_{18}H_{16}N_5O_4V$
Formula weight	1793.45	434.32	417.30
T [K]	100(2)	100(2)	100(2)
Wavelength [Å]	0.71073	0.71073	0.71073
Crystal system	monoclinic	triclinic	triclinic
Space group	$P2_1/c$	$P\bar{1}$	$P\bar{1}$
a [Å]	9.2529(3)	8.6178(18)	8.5358(4)
b [Å]	26.6010(8)	9.914(2)	10.2124(5)
c [Å]	7.3328(2)	11.942(2)	10.2489(5)
α [°]		70.921(9)	92.785(2)
β [°]	90.7120(10)	80.391(8)	90.016(2)
γ [°]		71.571(8)	106.312(2)
V [Å^3]	1804.73(9)	912.5(3)	856.34(7)
Z	1	2	2
F(000)	912	448	428
D_{calc} [g cm^{-3}]	1.650	1.581	1.618
μ [mm^{-1}]	0.821	0.585	0.618
θ [°]	1.53 to 26.49	1.81 to 27.60	2.49 to 27.60
R_{int}	0.0312	0.0392	0.1012
Crystal size [mm^3]	0.31 × 0.29 × 0.24	0.37 × 0.15 × 0.07	0.25 × 0.11 × 0.10
Goodness-of-fit on F^2	1.172	1.073	1.068
$R_1[I > 2\sigma(I)]$[a]	0.0320	0.0456	0.0361
wR_2 (all data)[b]	0.0973	0.1477	0.0971
Largest differences peak and hole (e Å^{-3})	0.666 and –0.476	0.688 and –0.543	0.665 and –0.501
	10	**11**	**12**
Formula	$C_{18}H_{18}N_5O_5V$	$C_{21}H_{23}N_4O_5V$	$C_{19}H_{21}N_4O_6V$
Formula weight	435.31	462.37	452.34
T [K]	100(2)	100(2)	100(2)
Wavelength [Å]	0.71073	0.71073	0.71073
Crystal system	triclinic	monoclinic	triclinic
Space group	$P\bar{1}$	$P2_1/n$	$P\bar{1}$
A [Å]	8.719(15)	7.4905(6)	11.3567(19)
B [Å]	10.041(17)	21.2776(17)	12.675(2)
C [Å]	12.12(2)	13.2842(10)	16.231(2)
α [°]	71.044(16)		85.962(8)
β [°]	80.690(17)	91.497(4)	89.740(8)
γ [°]	71.496(17)		76.594(8)
V [Å^3]	950(3)	2116.5(3)	2266.8(7)
Z	2	4	4
F(000)	448	960	936
$D_{calcd.}$ [g cm^{-3}]	1.522	1.451	1.325
M [mm^{-1}]	0.564	0.510	0.477
θ [°]	1.78 to 26.34	1.81 to 27.88	2.01 to 26.28
R_{int}	0.0432	0.0435	0.0662
Crystal size [mm^3]	0.35 × 0.24 × 0.21	0.34 × 0.22 × 0.20	0.44 × 0.33 × 0.18
Goodness-of-fit on F^2	0.937	1.064	1.024
$R_1[I > 2\sigma(I)]$ [a]	0.0552	0.0417	0.0923
wR_2 (all data) [b]	0.1842	0.1229	0.2714
Largest differences peak and hole (e Å^{-3})	0.598 and –0.618	0.698 and –0.553	2.619 and –0.896

[a] $R_1 = \Sigma||F_o| - |F_c||/\Sigma|F_o|$. [b] $wR_2 = \{\Sigma[w(||F_o|^2 - |F_c|^2|)^2]|/\Sigma[w(F_o^2)^2]\}^{1/2}$.

[V^{V}O(ap-inh)(OMe)(MeOH)] (14): Complex **14** was prepared similarly to **11** from complex **4**, yield: 0.35 g (74 %). $C_{20}H_{22}N_5O_5V$ (463.36): calcd. C 51.84, H 4.79, N 15.11; found C 50.9, H 5.3, N 15.3.

X-ray Crystal Structure Determination: Three-dimensional X-ray data were collected with a Bruker Kappa Apex CCD diffractometer at low temperature for **6**, **7**, **9**, **10**, **11** and **12**, by the ϕ–ω scan method. Reflections were measured from a hemisphere of data collected from frames, each of them covering 0.3° in ω. A total of 40180 for **6**, 25323 for **7**, 32645 for **9**, 5196 for **10**, 66677 for **11** and 49609 for **12**, reflections measured were corrected for Lorentz and polarization effects and for absorption by multi-scan methods based on symmetry-equivalent and repeated reflections. Of the total, 3449 for **6**, 3118 for **7**, 3369 for **9**, 1904 for **10**, 4078 for **11** and 5906 for **12**, independent reflections exceeded the significance level ($|F|/\sigma|F|$) > 4.0. After data collection, in each case an multi-scan absorption correction (SADABS)[44] was applied, and the structure was solved by direct methods and refined by full-matrix least-squares on F^2 data using SHELX suite of programs.[45] Hydrogen atoms were located in difference Fourier map and left to refine freely, except for C(4) in **6**, N(4), C(4) and C(11) in **7**, C(4) and C(6) in **9**, C(4) and C(6) in **10** and C(1M), C(2M), C(4) and C(6) in **11**, which were included in calculation position and refined in the riding mode. In **7**, hydrogen atoms of water were located in the difference Fourier map and fixed to the relevant oxygen atom. In **10**, it was only possible to locate a hydrogen atom of water molecule due to the other hydrogen atom must be involved in symmetry operations. In **12**, all hydrogen atoms were included in the calculation position and refined in the riding mode. Refinements were done with allowance for thermal anisotropy of all non-hydrogen atoms. A final difference Fourier map showed no residual density outside: 0.666 and –0.476 e Å^{-3} for **6**, 0.688 and –0.543 for **7** e Å^{-3}, 0.665 and –0.501 e Å^{-3} for **9**, 0.598 and –0.618 e Å^{-3} for **10**, and 0.698 and –0.553 e Å^{-3} for **11**. In **12**, an important residual density of 2.619 and –0.896 e Å^{-3}, next to C(25), cannot be refined. A weighting Scheme $w = 1/[\sigma^2(F_o^2) + (0.057400\ P)^2 + 0.845800\ P]$ for **6**, $w = 1/[\sigma^2(F_o^2) + (0.085800\ P)^2 + 0.497200\ P]$ for **7**, $w = 1/[\sigma^2(F_o^2) + (0.044900\ P)^2 + 0.603500\ P]$ for **9**, $w = 1/[\sigma^2(F_o^2) + (0.102400\ P)^2 + 0.00000\ P]$ for **10**, $w = 1/[\sigma^2(F_o^2) + (0.068600\ P)^2 + 0.888100\ P]$ for **11** and $w = 1/[\sigma^2(F_o^2) + (0.148600\ P)^2 + 9.733800\ P]$ for **12**, where $P = (|F_o|^2 + 2|F_c|^2)/3$, were used in the latter stages of refinement. Further details of the crystal structure determination are given in Table 9.

CCDC 1470642 (for **6**), 1470643 (for **7**), 1470644 (for **9**), 1470645 (for **10**), 1470646 (for **11**), and 1470647 (for **12**) contain the supplementary crystallographic data for this paper. These data can be obtained free of charge from The Cambridge Crystallographic Data Centre.

Peroxidase Mimetic Activity

Catalytic Oxidation of Pyrogallol: To investigate the peroxidase-like activity of [V^{V}OL(OMe)(MeOH)]-type complexes, the catalytic oxidation of a peroxidase substrate, pyrogallol, with H_2O_2 was studied. The activity was determined using UV/Vis absorption spectrophotometry to monitor reaction progress by registering increases in absorbance at 420 nm (due to the formation of purpurogallin) within 1 h. First, a 0.025 M solution of 30 % H_2O_2 (1 mL), 0.025 M pyrogallol solution and catalyst [0.00010 g of V^{V}O(ap-fah)-(OMe)(MeOH)] (**12**) were added in phosphate buffer (3 mL, 1 M, pH 7.0) and the maximum measurable absorbance was recorded. Various parameters, such as amounts of oxidant and catalyst were optimized to identify reaction conditions enabling optimized oxidation of pyrogallol.

Kinetic measurements were carried out in time course mode by monitoring absorbance changes at 420 nm for 5 min and by varying the concentration of pyrogallol (0.20–2.2 mM) for a fixed concentration of H_2O_2 (0.00025 M) in the presence of the catalyst **12** (0.0010 g). Initial rates were calculated from the slope of the plot of absorbance vs. time over a period of 5 min and fitted to the Michaelis–Menten equation. Lineweaver–Burk linearizations were carried out using Origin 8.0 to calculate kinetic parameters such as maximal velocity (V_{max}) and turnover numbers (k_{cat}) from nonlinear curve fitting.

Catalytic Oxidation of 1-phenylethanol: Catalytic oxidative activities of synthesized vanadate complexes were screened in the oxidation of 1-phenylethanol for which monoxidovanadium(V) complexes **11**–**14** were used. In a typical reaction, 1-phenylethanol (1.2 g, 0.010 mol) and 30 % aqueous H_2O_2 (2.3 g, 0.020 mol) were mixed in CH_3CN (5 mL) followed by addition of catalyst (0.0010 g). The reaction mixture was slowly stirred at 80 °C for 6 h. For each reaction the oxidative product, acetophenone, was quantitatively detected using gas chromatography and its identity confirmed by GC–MS.

Acknowledgments

M. R. M. thanks the Science and Engineering Research Board (SERB), the Government of India, New Delhi for financial support of the work (grant number EMR/2014/000529). B. S. is thankful to Indian Institute of Technology Roorkee (IIT Roorkee) for awarding a MHRD fellowship. I. C. thanks the financial support from the Portuguese Fundação do Ministério de Ciência e Tecnologia (FCT), project number UID/QUI/00100/2013 and the IST-UTL Centres of the Portuguese NMR spectroscopy.

Keywords: Bioinorganic chemistry · Enzyme mimics · Vanadium · Oxidation

[1] C. Regalado, B. E. García-Almendárez, M. A. Duarte-Vázquez, *Phytochem. Rev.* **2004**, *3*, 243–256.
[2] a) M. Sundaramoorthy, M. Gold, T. Poulos, *J. Inorg. Biochem.* **2010**, *104*, 683–690; b) J. Steinreiber, T. Ward, *Coord. Chem. Rev.* **2008**, *252*, 751–766.
[3] C. Leblanc, H. Vilter, J.-B. Fournier, L. Delage, P. Potin, E. Rebuffet, G. Michel, P. L. Solari, M. C. Feiters, M. Czjzek, *Coord. Chem. Rev.* **2015**, *301–302*, 134–146.
[4] D. Rehder, G. Santoni, G. M. Licini, C. Schulzke, B. Meier, *Coord. Chem. Rev.* **2003**, *237*, 53–63.
[5] D. Wischang, O. Brücher, J. Hartung, *Coord. Chem. Rev.* **2011**, *255*, 2204–2217.
[6] P. J. Deuss, R. den Heeten, W. Laan, P. C. J. Kamer, *Chem. Eur. J.* **2011**, *17*, 4680–4698.
[7] M. Á. Vázquez-Fernández, M. R. Bermejo, M. Fernández-García, G. González-Riopedre, M. J. Rodríguez-Doutón, M. Maneiro, *J. Inorg. Biochem.* **2011**, *105*, 1538–1547.
[8] Q. Wang, Z. Yang, X. Zhang, X. Xiao, C. K. Chang, B. Xu, *Angew. Chem. Int. Ed.* **2007**, *46*, 4285–4289; *Angew. Chem.* **2007**, *119*, 4363.
[9] S. P. de Visser, J. S. Valentine, W. Nam, *Angew. Chem. Int. Ed.* **2010**, *49*, 2099–2101; *Angew. Chem.* **2010**, *122*, 2143.
[10] Z. Dong, Q. Luo, J. Liu, *Chem. Soc. Rev.* **2012**, *41*, 7890–7908.
[11] Y. Murakami, J.-I. Kikuchi, Y. Hisaeda, O. Hayashida, *Chem. Rev.* **1996**, *96*, 721–758.
[12] H. Wei, E. Wang, *Anal. Chem.* **2008**, *80*, 2250–2254.
[13] N. Li, Y. Yan, B.-Y. Xia, J.-Y. Wang, X. Wang, *Biosens. Bioelectron.* **2014**, *54*, 521–527.
[14] a) N. D. Chasteen (Ed.), *Vanadium in Biological Systems*, Kluwer, Dordrecht, The Netherlands, **1990**; b) H. Sigel (Ed.), *Metal ions in Biologi-*

cal Systems Vanadium and its Role in Life, Marcel Dekker, New York, **1995**, vol. 31; c) A. S. Tracey, D. C. Crans (Eds.), *Vanadium Compounds: Chemistry, Biochemistry and Therapeutic Applications*, American Chemical Society, Washington, *DC*, **1998**.

[15] a) J. O. Nriagu (Ed.), *Vanadium in the Environment*, John Wiley & Sons, NewYork, **1998**; b) A. Butler, C. J. Carrano, *Coord. Chem. Rev.* **1991**, *109*, 61–105; c) H. Michibata, N. Yamaguchi, T. Uyama, T. Ueki, *Coord. Chem. Rev.* **2003**, *237*, 41–51; d) M. R. Maurya, *Coord. Chem. Rev.* **2003**, *237*, 163–181; e) D. Rehder, *Coord. Chem. Rev.* **1999**, *182*, 297–322; f) A. Butler, A. H. Baldwin, *Vanadium Bromoperoxidase and Functional Mimics*, in: *Structure and Bonding*, Springer, Berlin, Heidelberg, Germany, **1997**, vol. 89, p. 109–132.

[16] a) M. R. Maurya, N. Kumar, N. Chaudhary, *Polyhedron* **2015**, *97*, 103–111; b) M. R. Maurya, N. Chaudhary, F. Avecilla, I. Correia, *J. Inorg. Biochem.* **2015**, *147*, 181–192.

[17] a) N. A. Khalil, E. M. Ahmed, K. O. Mohamed, Y. M. Nissan, S. A. Zaitone, *Bioorg. Med. Chem.* **2014**, *22*, 2080–2089; b) G. Saidachary, K. V. Prasad, D. Divya, A. Singh, U. Ramesh, B. Sridhar, B. C. Raju, *Eur. J. Med. Chem.* **2014**, *76*, 460–469; c) A. K. El-Sawaf, A. A. Fatah Nassar, El.-S. El-Samanody, *Sci. J. Chem.* **2014**, *2*, 17–26; d) N. Raman, A. Selvan, P. Manisankar, *Spectrochim. Acta Part A* **2010**, *76*, 161–173.

[18] M. R. Maurya, N. Saini, F. Avecilla, *RSC Adv.* **2016**, *6*, 12993–13009.

[19] G. Tojo, M. Fernandez, *Oxidation of Alcohols to Aldehydes and Ketones: A Guide to Current Common Practice*, Springer, New York, **2007**.

[20] K. Elvingson, A. Gonzáles-Baró, L. Pettersson, *Inorg. Chem.* **1996**, *35*, 3388–3393.

[21] M. M. Hänninen, A. Peuronen, P. Damlin, V. Tyystajärvi, H. Kivelä, A. Lehtonen, *Dalton Trans.* **2014**, *43*, 14022–14028.

[22] a) P. Adão, M. R. Maurya, U. Kumar, F. Avecilla, R. T. Henriques, M. L. Kusnetsov, J. Costa Pessoa, I. Correia, *Pure Appl. Chem.* **2009**, *81*, 1279–1296; b) I. Correia, J. Costa Pessoa, M. T. Duarte, R. T. Henriques, M. F. M. Piedade, L. F. Veiros, T. Jakusch, T. Kiss, Á. Dörnyei, M. M. C. A. Castro, C. F. G. C. Geraldes, F. Avecilla, *Chem. Eur. J.* **2004**, *10*, 2301–2317.

[23] a) D. Rehder, *Bioinorganic Vanadium Chemistry*, Wiley, Chichester, UK, **2008**; b) D. Rehder, C. Weidemann, A. Duch, W. Priebsch, *Inorg. Chem.* **1988**, *27*, 584–587.

[24] a) N. F. Choudhary, P. B. Hitchcock, G. J. Leigh, *Inorg. Chim. Acta* **2000**, *310*, 10–20; b) P. Adão, J. Costa Pessoa, R. T. Henriques, M. L. Kuznetsov, F. Avecilla, M. R. Maurya, U. Kumar, I. Correia, *Inorg. Chem.* **2009**, *48*, 3542–3561.

[25] a) B. Ilhan-Ceylana, E. Tuzunb, Y. Kurta, M. Acikgozc, S. Kahramand, G. Atunb, B. Ulkusevena, *J. Sulfur Chem.* **2015**, *36*, 434–449; b) M. Chatterjee, S. Ghosh, B. M. Wu, T. C. M. Wak, *Polyhedron* **2006**, *17*, 1369; c) J. E. Kuder, H. W. Gibson, D. Wychick, ***J.** Org. Chem.* **1975**, *40*, 875–879; d) S. Mohebbi, B. Bakhshi, *J. Coord. Chem.* **2008**, *61*, 22615–2628.

[26] C. Das, P. Adak, S. Mondal, R. Sekiya, R. Kuroda, S. I. Gorelsky, S. K. Chattopadhyay, *Inorg. Chem.* **2014**, *53*, 11426–11437.

[27] Y. Kurt, B. Ilhan-Ceylan, M. Açıkgöz, E. Tüzün, G. Atun, B. Ülküseven, *Polyhedron* **2013**, *65*, 67–72.

[28] M. Mandal, V. Nagaraju, G. V. Karunakar, B. Sarma, B. Jyoti, B. Kusum, K. Bania, *J. Phys. Chem. C* **2015**, *119*, 28854–28870.

[29] T. L. Riechel, D. T. Sawyer, *Inorg. Chem.* **1975**, *14*, 1869–1875.

[30] T. B. Karpishin, T. M. Dewey, K. N. Raymond, *J. Am. Chem. Soc.* **1993**, *115*, 1842–1851.

[31] S. P. Dash, S. Majumder, A. Banerjee, M. Fernanda, N. N. Carvalho, P. Adão, J. Costa Pessoa, K. Brzezinski, E. Garribba, H. Reuter, R. Dinda, *Inorg. Chem.* **2016**, *55*, 1165–1182.

[32] A. Rockenbauer, L. Korecz, *Appl. Magn. Reson.* **1996**, *10*, 29–43.

[33] K. Wurthrich, *Helv. Chim. Acta* **1965**, *48*, 1012–1017.

[34] N. D. Chasteen, J. Reuben (Eds.), in: *Biological Magnetic Resonance*, Plenum, New York, **1981**, p. 53–119.

[35] a) J. Benitez, L. Becco, I. Correia, S. M. Leal, H. Guiset, J. Costa Pessoa, J. Lorenzo, S. Tanco, P. Escobar, V. Moreno, B. Garat, D. Gambino, *J. Inorg. Biochem.* **2011**, *105*, 303–313; b) S. Gorelsky, G. Micera, E. Garribba, *Chem. Eur. J.* **2010**, *16*, 8167–8180.

[36] D. Feng, Z.-Y. Gu, J.-R. Li, H.-L. Jiang, Z. Wei, H.-C. Zhou, *Angew. Chem. Int. Ed.* **2012**, *51*, 10307–10310; *Angew. Chem.* **2012**, *124*, 9401.

[37] M. R. Maurya, N. Saini, F. Avecilla, *Inorg. Chim. Acta* **2015**, *438*, 168–178.

[38] M. R. Maurya, N. Saini, F. Avecilla, *Polyhedron* **2015**, *90*, 221–232.

[39] S. Kodama, Y. Ueta, J. Yoshida, A. Nomoto, S. Yano, M. Ueshimaa, A. Ogawa, *Dalton Trans.* **2009**, 9708–9711.

[40] K. Marui, Y. Higashiura, S. Kodama, S. Hashidate, A. Nomoto, S. Yano, M. Ueshima, A. Ogawa, *Tetrahedron* **2014**, *70*, 2431–2438.

[41] R. A. Rowe, M. M. Jones, *Inorg. Synth.* **1957**, *5*, 113–116.

[42] R. Verma, P. Chawla, S. K. Saraf, *Pharm. Sin.* **2012**, *3*, 546–555.

[43] N. P. Moorjani, K. M. Vyas, R. N. Jadeja, *J. Pure Appl. Sci.* **2010**, *18*, 68–72.

[44] G. M. Sheldrick, *SADABS*, version 2.10, University of Göttingen, Germany, **2004**.

[45] SHELX: G. M. Sheldrick, *Acta Crystallogr., Sect. A* **2008**, *64*, 112–122.

Received: April 12, 2016
Published Online: August 11, 2016

